Taylor & Francis
Taylor & Francis Group

ORIGINAL RESEARCH

⛔ OPEN ACCESS   ⟳ Check for updates

Tertiary lymphoid structure-related immune infiltrates in NSCLC tumor lesions correlate with low tumor-reactivity of TIL products

Suzanne M. Castenmiller[a,b]*, Nandhini Kanagasabesan[a,b]*, Aurélie Guislain[a,b], Benoît P. Nicolet[a,b], Marleen M. van Loenen[a], Kim Monkhorst[c], Alexander A.F.A. Veenhof[d], Egbert F. Smit[e,f], Koen J. Hartemink[d], John B.A.G. Haanen[g,h,i], Rosa de Groot[a,j], and Monika C. Wolkers ![ORCID][a,b]

aSanquin Blood Supply, Division Research Immunotherapy, and Landsteiner Laboratory and Department of Experimental Immunology, Amsterdam University Medical Center, Amsterdam, Netherlands; bOncode Institute, Utrecht, The Netherlands; cDepartment of Pathology, Netherlands Cancer Institute-Antoni van Leeuwenhoek Hospital (NKI-AvL), Amsterdam, The Netherlands; dDepartment of Surgery, Netherlands Cancer Institute-Antoni van Leeuwenhoek Hospital (NKI-AvL), Amsterdam, The Netherlands; eDepartment of Thoracic Oncology, Netherlands Cancer Institute-Antoni van Leeuwenhoek Hospital (NKI-AvL), Amsterdam, The Netherlands; fDepartment of Pulmonology, Leiden University Medical Center (LUMC), Leiden, The Netherlands; gDivision of Medical Oncology and Division of Molecular Oncology and Immunology, Netherlands Cancer Institute-Antoni van Leeuwenhoek Hospital (NKI-AvL), Amsterdam, The Netherlands; hDepartment of Medical Oncology, Leiden University Medical Center (LUMC), Leiden, The Netherlands; iHead of Melanoma Clinic, Centre Hospitalier Universitaire Vaudois (CHUV), Lausanne, Switzerland; jDepartment of Hematology, LUMC, Leiden, The Netherlands

ABSTRACT

Adoptive transfer of tumor infiltrating lymphocytes (TIL therapy) has proven highly effective for treating solid cancers, including non-small cell lung cancer (NSCLC). However, not all patients benefit from this therapy for yet unknown reasons. Defining markers that correlate with high tumor-reactivity of the autologous TIL products is thus key for achieving better tailored immunotherapies. We questioned whether the composition of immune cell infiltrates correlated with the tumor-reactivity of expanded TIL products. Unbiased flow cytometry analysis of immune cell infiltrates of 26 early-stage and 20 late-stage NSCLC tumor lesions was used for correlations with the T cell differentiation and activation status, and with the expansion rate and anti-tumor response of generated TIL products. The composition of tumor immune infiltrates was highly variable between patients. Spearman's Rank Correlation revealed that high B cell infiltration negatively correlated with the tumor-reactivity of the patient's expanded TIL products, as defined by cytokine production upon exposure to autologous tumor digest. In-depth analysis revealed that tumor lesions with high B cell infiltrates contained tertiary lymphoid structure (TLS)-related immune infiltrates, including BCL6$^+$ antibody-secreting B cells, IgD$^+$BCL6$^+$ B cells and CXCR5$^+$BLC6$^+$ CD4$^+$ T cells, and higher percentages of naïve CD8$^+$ T cells. In conclusion, the composition of immune cell infiltrates in NSCLC tumors associates with the functionality of the expanded TIL product. Our findings may thus help improve patient selection for TIL therapy.

Introduction

Adoptive cellular therapy with tumor infiltrating lymphocytes (TILs) has shown high potential for the treatment of solid tumors.[1] The exciting findings from small-scale phase I trials for advanced melanoma patients receiving TIL therapy[2–6] were recently confirmed in a phase III clinical trial,[7] revealing the great treatment potential of TIL therapy for metastasized melanoma patients. Importantly, and as previously suggested by a small-scale study,[8] this multi-center open-label trial demonstrated that not only treatment-naïve patients responded to TIL therapy. It also showed efficacy in patients that were resistant to checkpoint inhibitors.[7]

Owing to these successes, the generation of tumor-reactive TIL products has been assessed for other solid tumors, including bladder cancer,[9] ovarian cancer,[10] and renal cell cancer.[11] Additionally, we and others showed that TIL products

generated from treatment-naïve non-small cell lung cancer (NSCLC)-patients contain poly-functional tumor-reactive T cell products.[12,13] As for melanoma alike,[7,8] we found tumor-reactive T cells also in TIL products from late-stage pretreated NSCLC patients, indicating that TIL therapy could potentially be broadly applicable to NSCLC patients.[14] In line with these findings, a first very promising phase I clinical trial with TIL therapy in PD1-refractory patients recently reported a reduced tumor burden in most patients.[15] Consequentially, more clinical trials with TIL therapy are expected to start in the near future.[16,17]

However, similar to treatments with checkpoint inhibitors,[18–21] not all patients respond equally well to TIL therapy. For metastatic melanoma, 10–20% of the patients undergo long-term complete remission.[6,10] Others, however, undergo only partial remission or stable disease, or do not

benefit from TIL therapy at all.[4,6,7,15,22] To date, reports on indicators that stratify patients with a high likelihood to generate tumor-reactive TIL products are scarce. Such prediction tools are thus in high demand, as they will help select the patients who will benefit most from TIL therapy.

The divergent response rate to treatment with checkpoint inhibitors has been attributed to the immune cell composition of the tumor microenvironment (TME).[21,23,24] In particular high percentages of B cell infiltrates, and the presence of tertiary lymphoid structures (TLS) have been indicated as positive indicators of responding to checkpoint inhibitors.[23,25] Also for TIL therapy, first indications have been collected to study the influence of the TME composition on generating TIL products. In melanoma patients, the T cell differentiation status was proposed to correlate with the efficacy of the TIL product,[5,26] and in a small cohort, a correlation with the activation status of macrophages and dendritic cells was observed.[27] For NSCLC-derived TIL products, such correlations with the immune cell infiltrates in tumor lesions have, to our knowledge, not yet been reported. We hypothesized that studying the immune cell compartment in NSCLC tumor digests at baseline could potentially provide important insights into the quality and tumor-reactivity of expanded TIL products.

In this study, we mapped the immune cell infiltrates from 26 treatment-naïve early-stage and from 20 pre-treated late-stage NSCLC patients. Lymphoid cells were enriched in most tumor-specific immune infiltrates. Yet, we observed a high inter-patient variation. Notably, whereas NKT cells and neutrophils positively correlated with tumor-reactive T cells in expanded TIL products, B cells and conventional CD4^{+} T cells displayed a negative correlation. In particular, tumors with high B cell infiltrates displayed immune infiltrates related to mature tertiary lymphoid structure (TLS). We therefore postulate that mature TLS-related immune infiltrates negatively impact the tumor-reactivity potential of expanded TIL products.

Results

Tumor lesions display an influx of lymphoid cells, irrespective of the disease stage

To study the composition of immune cell infiltrates in NSCLC tumor lesions, we collected tumor and adjacent lung tissue from 26 early-stage, treatment-naïve patients, and metastatic tumor lesions from 20 late-stage NSCLC patients. Late-stage patients had different histories of treatment, including chemotherapy, immunotherapy, chemo-immuno combination therapy, or small-molecule inhibitor therapy (EGFR and ALK inhibitors; Table 1). 27 female and 19 male patients between 37 and 87 years of age (mean 63.2 years) were included, of which 37 patients (78%) had a history of smoking. Tumor size ranged from 0.7–8 cm^2, with an average of 3.5 cm^2 (Table 2).

We obtained more viable cells per gram tissue from enzymatically digested early-stage tumor lesions (32.3×10^6 $\pm23.8\times10^6$) than from the paired adjacent lung tissue (16.0×10^6 $\pm25.3\times10^6$, $p = 0.0013$; Table 2, Figure 1(a),

supplemental figure S1A). Tissue digests from late-stage tumors contained comparable numbers of viable cells per gram tissue cell to early-stage tumors (34.1×10^6 $\pm34.6\times10^6$; Table 2, Figure 1(a)). The lung digest contained higher percentages of CD45$^+$ immune cell infiltrates ($29.6\% \pm 18.5\%$) than both early- and late-stage tumors ($21.4\% \pm 20.0\%$ and $16.0\% \pm 20.1\%$, respectively; $p = 0.024$; Figure 1(b)). Nevertheless, the number of CD45$^+$ cells isolated per gram tissue was similar from lung and tumor digests (Figure 1(c)).

To define the percentage of lymphoid (T cell, B cell, NK cell, NKT cell) and myeloid (neutrophil, monocyte, dendritic cell) infiltrates, we performed an integrated multi-parameter flow cytometry analysis followed by a multistep analysis in R as described in the methods section (Table 3, supplemental figure S1, supplemental figure S2A). CD45$^+$ immune cells that could not be attributed to one specific cell subset based on the antibody panel we used (Table 3) were defined as 'unclassified'. The percentage of unclassified CD45$^+$ cells (which should include e.g. basophils, mast cells, eosinophils and possibly MAIT cells) was substantially reduced in early-stage tumor lesions compared to lung tissue, a feature that was not sustained in late-stage tumors (Figure 1(d,g)). Overall, early- and late-stage tumor lesions were more alike than early-stage tumors with the paired lung tissue (Figure 1(d)). In accordance with previous studies,[28,29] we found an increase of T cells and B cells in tumor lesions, at the cost of myeloid and NK cell infiltrates in the tumor lesions (Figure 1(d–h)).

Importantly, we observed a high interpatient variability in immune infiltrate composition (Figure 1(e–h)). For example, the interquartile range of B cell infiltrates in late-stage tumors ranged from 3.4% to 10.3% (Figure 1(g)), but it could be as little as 0.3% and as much as 44.6% in patients. Similarly, neutrophil infiltration ranged from 0.1% to 33.8%. Thus, tumor lesions display increased T and B cell infiltrates compared to healthy lung, yet the overall composition of immune infiltrates in NSCLC tumor lesions is highly variable between patients, irrespective of their disease stage.

B cell tumor infiltration positively correlates with CD4$^+$ conventional T cell infiltrates

Because immune cell infiltrates communicate with each other,[24] we examined how the presence of one immune cell subset related with that of others, using the Spearman's correlation coefficient (r_s). We first examined the lung and tumor lesions individually (supplemental figure S2). For lung tissue, CD8$^+$ T cell infiltrates positively correlated with the presence of Tregs and DCs (supplemental figure S2B,C). Early- and late-stage tumor lesions also displayed some correlations between immune cell infiltrates (supplemental figure S2D–G). To define correlations of immune infiltrates common to early- and late-stage tumors, we combined the two NSCLC cohort. In particular the positive correlation between neutrophil and monocyte infiltrates ($r_s = 0.35$, $p = 0.017$) and between B cell and conventional CD4$^+$ T cell infiltrates ($r_s = 0.43$, $p = 0.0042$) was conserved (Figure 2(a,b); supplemental figure S2H), suggesting a tumor-intrinsic correlation between different NSCLC-infiltrating immune cell subsets.

Table 1. Patient cohort.

Patient ID	Published	Age years	Gender M/F	Smoking cigarettes/day	Clinical stage [a] TNM7/TNM8	Patient outcome SD/PD/D	Tumor size cm²	Treatment	Met. Location
12	*12	70	F	yes (20/d)	IIB	D	5,6	naive	-
13	*12	57	F	yes (8/d)	IA	SD	1,7	naive	-
14	*12	37	F	yes (20/d)	IA	PD	2,3	naive	-
16	*12	63	F	yes (20/d)	IIB	SD	4,9	naive	-
17	*12	69	F	yes (10/d)	IB	D	2,7	naive	-
18	*12	56	F	yes (6/d)	IB	SD	3,5	naive	-
19	*12	79	F	yes (5/d)	IB	SD	4,2	naive	-
20	*12	73	M	yes (30/d)	IIIA	SD	8	naive	-
21	*12	51	F	yes (8/d)	IA	PD	2,7	naive	-
23	*12	61	M	yes (10/d)	IA3	SD	2,3	naive	-
25	*12	69	M	yes (20/d)	IA	D	2,3	naive	-
30		80	M	no (never)	IIIB	D	4,8	naive	-
31		71	M	yes (8/d)	IB	PD	3,7	naive	-
32		74	F	no (never)	IA	SD	2,6	naive	-
33		72	M	yes (25/d)	IIB	SD	1,7	naive	-
38		59	F	yes (40/d)	IIIB	D	5,7	naive	-
40		66	F	yes (5/d)	IIIA	SD	4,2	naive	-
42		69	F	yes (8/d)	IA	PD	1,5	naive	-
46		65	M	yes (20/d)	IIB	PD	2,5	naive	-
47		65	F	yes (25/d)	IA	SD	1,8	naive	-
48		54	F	yes (6/d)	IIIB	D	5	naive	-
49		59	F	yes (18/d)	IIIA	D	1,5	naive	-
50		72	M	yes (20/d)	IA	SD	2,1	naive	-
51		72	M	yes (10/d)	IIB		5	naive	-
57		46	M	yes (13/d)	IIIA	SD	5,3	naive	-
60		72	F	yes (17/d)	IIA	SD	1,2	naive	-
IV_01	*14	64	M	yes (unknown)	IV	SD	4,7	Immuno	Lung
IV_02	*14	64	F	no (never)	IV	D	3,2	Chemo	Lung
IV_03	*14	45	M	unknown	IIIA	SD	1,5	Naive	Lymphnode
IV_06	*14	50	F	yes (20/d)	IV	PD	3,5	Immuno	Lymphnode
IV_07	*14	58	M	yes (6/d)	IV	PD	2,4	Immuno	Lung
IV_08	*14	57	F	no (never)	IV	PD	0,1	Immuno	Lung
IV_09	*14	55	M	no (never)	IV	PD	2,5	EGFR-inh	Lung
IV_11	*14	60	F	yes (13/d)	IV	D	1,2	Naive	Subcutaneous tissue
IV_12	*14	69	F	no (never)	IV	PD	4,6	EGFR-inh	Liver
IV_13	*14	53	M	no (never)	IV	D	3	ALK inh	Adrenal gland
IV_14	*14	70	F	yes (20/d)	IV	D	7,5	Chemo	Adrenal gland
IV_15	*14	66	M	unknown	IV	D	4,5	Chemo-immuno	Subcutaneous tissue
IV_16	*14	87	M	yes (8/d)	IV	D	7,5	ALK inh	Adrenal gland
IV_18	*14	60	M	yes (30/d)	IV	SD	7,1	Chemo-immuno	Spleen
IV_19	*14	47	F	yes (5/d)	IV	D	3,5	Immuno	Adrenal gland
IV_21	*14	40	F	yes (25/d)	IV	SD	1,7	Chemo-immuno	Adrenal gland
IV_25	*14	73	M	yes (10/d)	IV	D	3,7	Chemo	Adrenal gland
IV_27	*14	72	F	yes (5/d)	IV	D	1,2	Chemo	Lung
IV_28		64	F	yes (30/d)	IV	D	4,5	EGFR-inh	Lung
IV_30		73	F	yes (10/d)	IV	SD	2,2	Immuno	Lung

M = male, F = female, TNM = tumor, nodes and metastasis, SD = stable disease, PD = progressive disease, D = diseased.
[a]American Joint committee on Cancer: Lung Cancer Staging.
*12 De Groot, R. et al. Polyfunctional tumor-reactive T cells are effectively expanded from non-small cell lung cancers, and correlate with an immune-engaged T cell profile. Oncoimmunology 8, (2019).
*14 Castenmiller, S. M. et al. Effective generation of tumor-infiltrating lymphocyte products from metastatic non-small-cell lung cancer (NSCLC) lesions irrespective of location and previous treatments. Immuno-Oncology Technol. 15, 100090 (2022).

Divergent immune infiltrate composition does not show effects on TIL expansion

Successful TIL therapy requires sufficient expansion to achieve a clinical response.[2] To define whether the cellular composition of the tumor digest correlated with the capacity of TILs to expand *in vitro*, we used TIL expansion data we previously reported,[12,14] and complemented them with the analysis for tumors from newly recruited patients (Table 1). We observed no overt correlations of the percentage of immune infiltrates with the fold expansion rate during the pre-REP (first 10–13 days of expansion) and the REP phase (second 10–13 days of expansion), except from a slight negative correlation of conventional CD4$^+$ T cells with TIL expansion during the pre-REP phase (r_s=-0.35, $p = 0.031$; Figure 2(c,d)). We did not observe

any gender- or age-related correlations in terms of TIL expansion (supplemental figure S2I). Overall, the composition of immune infiltrates in digested tumor lesions had a limited effect on the TIL expansion from the same lesion.

B and NKT cell infiltrates in the TME correlate with tumor-reactivity of expanded TIL products

Another key objective for effective TIL therapy is the presence of tumor-reactive T cells in the expanded TIL product. We therefore questioned whether any immune cell type present in tumor digest correlated with tumor reactivity of the TIL products.[12,14] Tumor reactivity was defined by CD137 (4-1BB) expression, by the production of at least one of the key pro-

Table 2. TIL characteristics.

Patient ID	ex vivo						% of CD3 (tumor)			Expansion			postREP phenotype % of lymphocytes		T cell functionality %CD137		% Cytokines[b]	
	Tumor Cells/gram tissue	Lung Cells/gram tissue	Tumor %CD45	Lung %CD45	Tumor CD45/gram tissue	Lung CD45/gram tissue				preREP	REP	total	CD4	CD8	CD4	CD8	CD4	CD8
12	3,33E+06	2,50E+06	23	41,6	7,66E+05	1,04E+06	14,82	69,73	9,20			750	56,3	42,2			1,2	1,9
13	8,33E+07	1,33E+08	33,6	8,4	2,80E+07	1,12E+07	25,77	61,60	12,16	1.2	410	492	71,5	21,2	0,1	2,2	0,5	1
14	4,00E+06	1,64E+06	19,9	52,2	7,96E+05	8,56E+05	25,19	72,51	2,21	1	600	600	2,88	97,1	1,1	0,7	0,5	0,4
16	2,43E+07	1,80E+07	3,9	36,4	9,48E+05	6,55E+06	29,02	32,29	8,53	2.2	304	668.8	6,7	81,9	0	0	0,3	0,2
17	6,46E+06	1,26E+06	60	71,3	3,88E+06	8,98E+05				3.5	1250	4375	72,3	24,5	2,3	3	16	2,5
18	6,00E+06	6,00E+05	16,1	17,8	9,66E+05	1,07E+05	36,23	52,85	5,17	2.2	625	1375	44,1	49,6	1,9	1,3	0,5	0,8
19	6,40E+06	4,22E+06	24,4	38,4	1,56E+06	1,62E+06	52,48	32,80	10,51				60,5	37,3	4,6	2	2,4	1,9
20	9,26E+06	2,00E+06	0,5	16,3	4,63E+04	3,26E+05	48,28	23,21	10,29	1.5	675	1012.5	14,7	80,2	1,6	4,7	2,6	1,5
21	4,92E+07	1,78E+07	9	14	4,43E+06	2,49E+06	35,31	29,00	4,10	1	50	50	63,3	34,2	3,6	4,6	2,5	4,5
23	2,40E+07	2,00E+06	72,5	31,1	1,74E+07	6,22E+05	21,93	66,94	8,20									
25	5,35E+07	2,69E+07	71,3	42,3	3,81E+07	1,14E+07	42,17	44,74	10,00	1.3	50	65	59,1	35,4	1,8	6,4	1,2	1,6
30	4,92E+07	1,78E+07	14,9	36,4	7,32E+06	6,48E+06	13,80	61,08	11,05	2	400	800	45,7	14,1	4,3	1	1,8	0,5
31	5,82E+07	1,23E+07	26,6	28,9	1,55E+07	3,56E+06	30,24	53,34	9,51	2	125	250	29,0	21,4	4,7	2,8	0	0
32	1,50E+07	9,09E+06	25,9	29,8	3,89E+06	2,71E+06	21,83	53,04	0,31	2	500	1000	27,9	68,7	0	0,2	0	0
33	1,50E+07	2,86E+07	7,14	29,9	1,07E+06	8,54E+06	38,23	54,00	0,22	2	200	400	39,8	54,7	0,6	0,3	1	1,5
38	3,10E+07	1,33E+06	24,8	34,6	7,69E+06	4,60E+05	6,39	24,54	0,41	2	600	1200	41,3	40,3	1,1	2	1,6	38,7
40	3,20E+07	5,33E+06	2,3	32,6	7,36E+05	1,74E+06				2	160	320	10,3	56,5	0,3	0,2	0,4	0,9
42	2,29E+07	1,65E+07	20	19,2	4,58E+06	3,17E+06	5,34	54,45	4,40	2	500	1000	23,4	48,8	0,4	0,7	1,7	1,4
46	8,25E+07	2,50E+07	32,3		2,66E+07		48,11	28,44	6,42	10	30	300	23,8	54,8	1,5	3	0,5	0,1
47	6,07E+07	1,53E+07	1,3	6,2	7,89E+05	9,49E+05	3,65	18,88	0,20	1,1	20	22	54,3	13,3	0,2	0,4	0,1	0,2
48	2,57E+07	1,06E+07	2,4	62,7	6,17E+05	6,65E+06	4,67	31,40	2,09	5	230	1150	46,4	27,8	0,7	0,9	0,2	0,8
49	2,07E+07	2,00E+07	1,4	1,8	2,90E+05	3,60E+06	38,34	27,00	0,11	2	125	250	45,9	40	1	1	0,6	1,1
50	6,29E+07	6,15E+06	10,4	19,5	6,54E+06	1,20E+06	51,39	23,84	0,41	3	1300	3900	20,1	51,1	0,4	1,5	0,1	0,2
51	2,50E+07	1,75E+07	20	7,9	5,00E+06	1,38E+06	13,43	13,98	5,66	3	400	1200	2,2	24,9	6,9	3,2	5,1	0,9
57	4,87E+07	1,38E+07	6,9	56,6	3,36E+06	7,81E+06	31,90	29,45	0,37	20	20	400						
60	2,08E+07	7,30E+06	26,6	5,1	5,53E+06	3,72E+05	39,90	47,40	8,64	10	80	800						
IV_01	1,55E+07		5,9		9,15E+05		48,94	17,41	3,40	12	50	587	13,1	50,6	0,7	4,4	12,5	6,6
IV_02	3,76E+07		18		6,77E+06		28,20	42,08	21,62	6	37	212	91,5	6,1	0,3	1,7	3,9	4,2
IV_03	3,45E+07		40,6		1,40E+07		22,81	32,24	5,27	2	90	146	6,7	71,4	7,6	1,6	11,4	1,5
IV_06	6,67E+07		46,4		3,09E+07		35,31	41,11	14,19	66	59	3935	40,5	45,6	0	0	1,3	0
IV_07	1,59E+08		67,4		1,07E+08		60,28	23,79	15,35	181	22	3984	21,9	66,8	0	0,3	2,6	5,5
IV_08	2,75E+07		5,3		1,46E+06		12,46	30,05	2,40	67	124	8346	55,6	39,5	0	0	2,6	0
IV_09	7,60E+06		20,2		1,54E+06		19,48	34,32	14,74	26	11	277	16,4	71,3	2,1	2	3,4	2,5
IV_11	1,67E+07		0,3		5,00E+04		26,74	56,88	16,17	40	3	120						
IV_12	1,55E+07		1,1		1,71E+05		55,16	42,31	1,56	168	160	26827	9,9	78,3	1	1,4	2,2	1,2
IV_13	3,76E+07		3,2		1,20E+06		51,38	29,60	7,88				24,8	44,5	3,3	5,8	4,6	5,1
IV_14	5,58E+07		51,1		2,85E+07		11,97	46,19	20,30	13	44	579	48,3	38,5	1,6	0	7,5	3,9
IV_15	5,99E+06		1,9		1,14E+05		47,47	30,77	7,75	24	17	408	8,11	79	11,4	0,4	13,3	0,4
IV_16	3,37E+07		12,6		4,25E+06		84,00	14,31	1,69	6	28	177	51,7	43,4	10	2,1	10,1	2,5
IV_18	1,10E+07		1,2		1,32E+05		33,90	20,52	6,24	107	79	8382	29	50	0	0	1,8	1,6
IV_19	3,97E+07		0,5		1,98E+05		54,88	26,67	8,32	2	298	728	74,6	17,5	0,3	0	0	0,7
IV_21	1,05E+07		1,2		1,26E+05		44,11	37,52	4,06	9	24	212	50,8	42,1	10,4	14	11,9	4,4
IV_25	2,40E+07		0,1		2,40E+04		44,36	47,56	2,13	10	23	230						
IV_27	6,20E+07		27,1		1,68E+07		30,76	27,51	7,18	10	45	450						
IV_28	1,50E+07		8,1		1,22E+06		40,90	34,98	10,58	10	130	1300						
IV_30	7,00E+06		7		4,90E+05					12	120	1440						

REP: rapid expansion phase.
[b]Based on the production of at least one of the key cytokines (IFNγ, TNF, and/or IL-2).

inflammatory cytokines (IFNγ, TNF and IL-2) and the capacity to produce two or more cytokines simultaneously (polyfunctional T cells) upon exposure to autologous tumor digest for 6–7 hours (Table 2), as previously described.[12,14] The percentage of NKT cells in the TME positively correlated with CD137 expression on expanded CD4+ TILs ($r_s = 0.51$, $p = 0.0016$), and the percentage of neutrophils positively correlated with cytokine production of expanded CD4+ TILs ($r_s = 0.38$, $p = 0.019$) (Figure 2(e,f)). Notably, this positive correlation between neutrophils and cytokine production of CD4+ TILs was even more prominent, when we subdivided the samples into TIL cultures that were directly cultured (rs = 0.48, $p = 0.013$) compared to samples that were cryo-preserved ($n = 13$; Figure 2(f)). Surprisingly, however, the percentage of conventional CD4+ T cells in the TME negatively correlated with cytokine production of expanded CD4+ TILs (r_s=-0.38, $p = 0.022$) (Figure 2(e,f)). Even more prominently, the percentage of B cells in the TME negatively correlated with cytokine production by expanded CD8+ TILs (r_s=-0.47, $p = 0.0031$) (Figure 2(e,f)). A similar trend was observed for CD4+ TILs (Figure 2(e)). Lastly, the percentage of conventional CD4+ T cells in the TME negatively correlated with polyfunctional CD8 TILs (Figure 2(e,f)). Thus, TIL products that were generated from tumor lesions with high B cell and conventional CD4+ T cell infiltrates correlated with TIL products displaying lower percentages of tumor reactivity. Again, we did not observe any gender- or age-related correlations in terms of tumor reactivity (supplemental figure S2J). Of note, for a subset of this cohort (29 samples), we also measured the expression of CD107α, a degranulation marker (Figure 2(e)).

No significant correlations were observed between the immune infiltrate and CD107α expression on either CD4 or CD8 TILs after co-culture (Figure 2(e)).

Activation status of neutrophils negatively correlates with tumor-reactivity of TIL products

The activation status of TME infiltrates has been reported to influence the presence and functionality of tumor-reactive T cells,[30–33] a feature that was also reported for NSCLC.[29,34] PD-L1, which is expressed mainly on activated myeloid cells, but can also be found on lymphoid cells,[35,36] plays a key role in suppressing inflammatory immune responses.[37] Likewise, HLA-DR is expressed on activated antigen presenting cells such as DCs, monocytes and B cells, and on activated T cells.[34,38,39] We questioned whether the PD-L1 or HLA-DR expression on the immune infiltrates could explain the high variety of anti-tumor responses we observe in TIL products. In NSCLC infiltrates, DCs and monocytes displayed high percentages of PD-L1 and HLA-DR expression, irrespective of the disease stage (supplemental figure S3A, Figure 3(a,b)). B cells primarily showed high percentages of HLA-DR expression, again in both early- and late-stage tumors (Figure 3(a,b)). For all other cell types, the percentage of PD-L1 and HLA-DR expressing cells was more variable (Figure 3(a,b)). Of note, PD-L1 or HLA-DR expression on CD3^{+} T cell infiltrates did not correlate with increased Treg infiltration (supplemental figure S3B), indicating that PD-L1 or HLA-DR expression rather originated from conventional CD3^{+} T cells. The most prominent variation of PD-L1 and HLA-DR expression was observed for neutrophils (Figure 3(a,b)). Independently of the tumor stage, neutrophils showed very high, or very low expression of these two activation markers (Figure 3(a–c)). As for monocytes and DCs alike, PD-L1 or HLA-DR were by and large co-expressed (Figure 3(c)).

We next determined if PD-L1 or HLA-DR expression on immune cells corresponded with the composition of TME infiltrates. B cell infiltrates positively correlated with PD-L1 expression on NKT and T cell infiltrates (Figure 3(d), supplemental figure S3C). In contrast, neutrophil and monocyte infiltrates negatively correlated with PD-L1 expression on T cells, and neutrophils with the PD-L1 expression on neutrophils, NK cells and monocytes (Figure 3(d), supplemental figure S3C). The HLA-DR expression correlates with TME infiltrates were less pronounced, yet, neutrophil infiltrates negatively correlated with HLA-DR expression on NK cells and neutrophils (Figure 3(e), supplemental figure S3D). Thus, the presence of neutrophils in the TME negatively correlates with the immune activation status of other TME immune infiltrates.

We also studied whether the PD-L1 or HLA-DR expression on TME infiltrates correlated with the tumor-reactivity of expanded TILs. We found no effect of PD-L1 and HLA-DR expression on B or T cells with tumor reactivity (Figure 3(f,g)). In contrast, PD-L1-expressing DCs in the TME positively correlated with CD137 expression on expanded CD4^{+} and CD8^{+} TILs (Figure 3(f), supplemental figure S3E), suggesting that the presence of activated DCs points to the presence of tumor-reactive T cells. Interestingly, PD-L1 and HLA-DR expression on neutrophils negatively correlated with cytokine

expression of tumor-exposed expanded TILs (Figure 3(f,g); supplemental figure S3E,F). Thus, not only the overall presence of neutrophils in NSCLC tumors negatively correlates with the percentage of tumor-reactive T cells in TIL products, but also their PD-L1 and HLA-DR expression levels.

B cell infiltrates correlate with T cell differentiation status and are indicative of mature tls-related immune infiltrates

Previous studies proposed that the T cell differentiation status in melanoma patients correlated with the efficacy of TIL therapy.[5,26] Also in NSCLC patients, the T cell differentiation status can greatly vary.[40] To determine whether the T cell differentiation status correlated with the tumor-reactivity of expanded TILs, we measured the percentage of naïve T cells (Tn), central memory T cell (Tcm), effector memory cells (Tem), and terminally differentiated effector T cells (Temra) *ex vivo*, based on CD27 and CD45RA expression for all 46 NSCLC patients (supplemental figure S4A; Table 2). Naïve CD4^{+} and CD8^{+} T cells correlated negatively with CD137 expression and with cytokine expression of expanded TIL products (Figure 4(a), supplemental figure S4B), suggesting that high levels of naïve T cells in the TME result in inferior tumor reactivity of the TIL products. Central memory CD8^{+} T cells negatively correlated with polyfunctional CD8 TILs (Figure 4(a), supplemental figure S4B). Interestingly, B cell infiltrates positively correlated with the presence of naïve CD8^{+} and CD4^{+} T cells, at the expense of effector memory T cells (Figure 4(b), supplemental figure S4C). Combined with the observation that B cell infiltrates positively correlated with CD4^{+} T cell infiltrates (Figure 2(a)), but negatively correlated with tumor-reactive T cells in the expanded TIL product (Figure 2(e)), we hypothesized that increased B cell infiltration indicates recruitment of naïve bystander T cells, a feature that is observed in the presence of TLS.[41–43] This could then possibly alter the ratio of bystander naïve T cells and effector T cells containing the tumor reactive T cell population, and thus create a different, inferior, starting condition for the generation of TIL products (Figure 4(c)).

To test this hypothesis, we used the still available tumor digest of 2 patients with a low and 2 patients with a high percentage of B cell infiltrates for this analysis, because it is the starting material for generating TIL products. We profiled tumor-infiltrating B cells and CD4^{+} T cells in detail. Intriguingly, tumors with high B cell infiltrates contained higher percentages of class-switched IgG^{+} and IgA^{+} expressing B cells, and very low percentages of naïve IgM[+]IgD^{+} B cells (Figure 5(a,b)). Tumors with high B cell infiltrates also contained more antibody secreting cells (ASC), with an increased population of CD138^{+} ASCs, which is indicative of the presence of follicle formation and plasma cells[43] (Figure 5(b)). IgD^{+} B cells were almost exclusively present in tumors with high B cell infiltration (Figure 5(b)).

We also measured the BCL6 expression in the tumor digest of 2 patients with a low and 2 patients with a high percentage of B cell infiltrates.[44] BCL6 expression was in particular found on CD38^{+} ASCs (Figure 5(c,d)), and co-expression of CD38 and BCL6 identifies germinal center (GC) B cells.[44] Interestingly, BCL6 expression was also substantially elevated in IgD^{+} B cells

Table 3. Detailed antibody panels.

Panel	Marker	Fluorochrome	Dilution	Clone	Manufacturer
Immune cell composition	CD45	BUV805	800	HI30	BD
	CD19	BUV 737	400	SJ25C1	BD
	CD20	BUV 737	100	2H7	BD
	CD16	BUV 496	200	3G8	BD
	CD1a	BUV 395	100	HI149	BD
	CD15	BV605	800	W6D3	Biolegend
	CD3	BV510	200	SK7	Biolegend
	CD11b	BV421	200	ICRF44	Biolegend
	CD11C	PerCp-Cy5.5	50	3.9	Biolegend
	HLA-DR	FITC	200	L23(G46-6)	BD
	CD14	PECy7	200	63D3	Biolegend
	CD274 PDL-1	PE	50	29E.2A3	Biolegend
	live/dead	APC/Cy7	1000		Thermofisher/Invitrogen
	CD33	Alx700	100	WM53	BD
	CD68	APC	25	Y1/82A	Biolegend
T cell phenotype	CD3	PerCp-Cy5.5	100	SK7	Biolegend
	PD-1	FITC	100	EH12-2H7	Biolegend
	CD56	BV605	100	HCD56	Biolegend
	CD27	BV510	200	O323	Biolegend
	CD127	BV421	100	A019D5	Biolegend
	CD8	BUV805	500	SK1	BD
	CD45RA	BUV 737	200	HI100	BD
	CD4	BUV 496	200	SK3	BD
	CD69	BUV395	100	FN50	BD
	Live/dead	APC-Cy7	800		Thermofisher/Invitrogen
	CD45RO	Alx700	50	UCHL1	Biolegend
	FOXP3	ALX 647	25	259D	Biolegend
	CD103	PE-Cy7	200	Ber-ACT8	Biolegend
	CD25	PE	25	BC96	Biolegend
Tumor reactivity	CD3	PerCP-cy5.5	100	SK7	Biolegend
	IL2	Alx488	100	MQ1-17H12	Biolegend
	TNF	BV785	200	Mab11	Biolegend
	CD154	BV510	100	24-31	Biolegend
	PD-1	BV421	100	EH12.1	BD
	CD8	BUV805	500	SK1	BD
	CD4	BUV496	100	SK3	BD
	CD107a	BUV395	100	H4A3	BD
	Live/dead	APC-Cy7	1000		Thermofisher/Invitrogen
	CD137	Alx647	100	4B4-1	Thermofisher/Invitrogen
	IFNg	PE	800	4S.B3	Biolegend
B cell and Tfh phenotype in TME	CD11c	PerCP	100	3.9	Biolegend
	IgG	BB515	100	G18-145	BD
	CD27	BV650	200	L128	BD
	IgM	BV605	100	MHM-88	Biolegend
	CD3	BV510	100	SK7	Biolegend
	CD19	BV421	75	SJ25C1	Biolegend
	CD21	BUV805	100	1048	BD
	CD138	BUV737	100	MI15	BD
	CD4	BUV661	100	SK3	BD
	CD38	BUV496	100	HIT2	BD
	CD24	BUV395	100	ML5	BD
	Live/dead	APC-cy7	1000		Thermofisher/Invitrogen
	IgD	AF647	75	IA6-2	BD
	IgA	PE	3000	2052-09	Southern-Biotech
	CXCR5	PE-Dazzle594	100	J252D4	Biolegend
	BCL6	PE-Cy7	400	7D1	Biolegend

(Figure 5(c,d)), which identifies mantle zone B cells, typically found at the border of TLS.[44] Concomitant with this finding, tumor lesions with high B cell infiltrates also contained CXCR5$^+$ CD4$^+$ follicular helper T cells[45,46] (Tfh, $n = 3$) (Figure 5(e,f)), with percentages that were comparable to what was previously reported for tumor infiltrates.[47,48] Moreover, Tfh cells were undetectable in poorly B-cell infiltrated tumors (Figure 5(e,f)). Importantly, BCL6 expression was exclusively detected in CXCR5$^+$ CD4$^+$ T cells, but not on CXCR5$^-$ conventional CD4$^+$ T cells (Figure 5(f)), further consolidating that CXCR5$^+$ CD4$^+$ T cells are bona fide Tfh cells.[49] Lastly, in line with the correlation plots (Figure 4(b)), tumors with high B cell infiltration contained higher percentages of

naïve CD4$^+$ and CD8$^+$ T cells (Figure 5(f)). Thus, we conclude that high B cell infiltrates in NSCLC tumors indicate the presence of GC B cells, mantle zone B cells, Tfh cells and naïve CD4$^+$ and CD8$^+$ T cells. This, in turn, negatively correlates with the tumor reactivity of expanded TIL products.

Discussion

The immune cell composition of the tumor microenvironment is a strong indicator for survival of cancer patients,[23–25] which can influence the success rate of immune checkpoint blockade therapies.[50–53] Here, we show that the tumor-reactivity of expanded TIL products from NSCLC tumors negatively
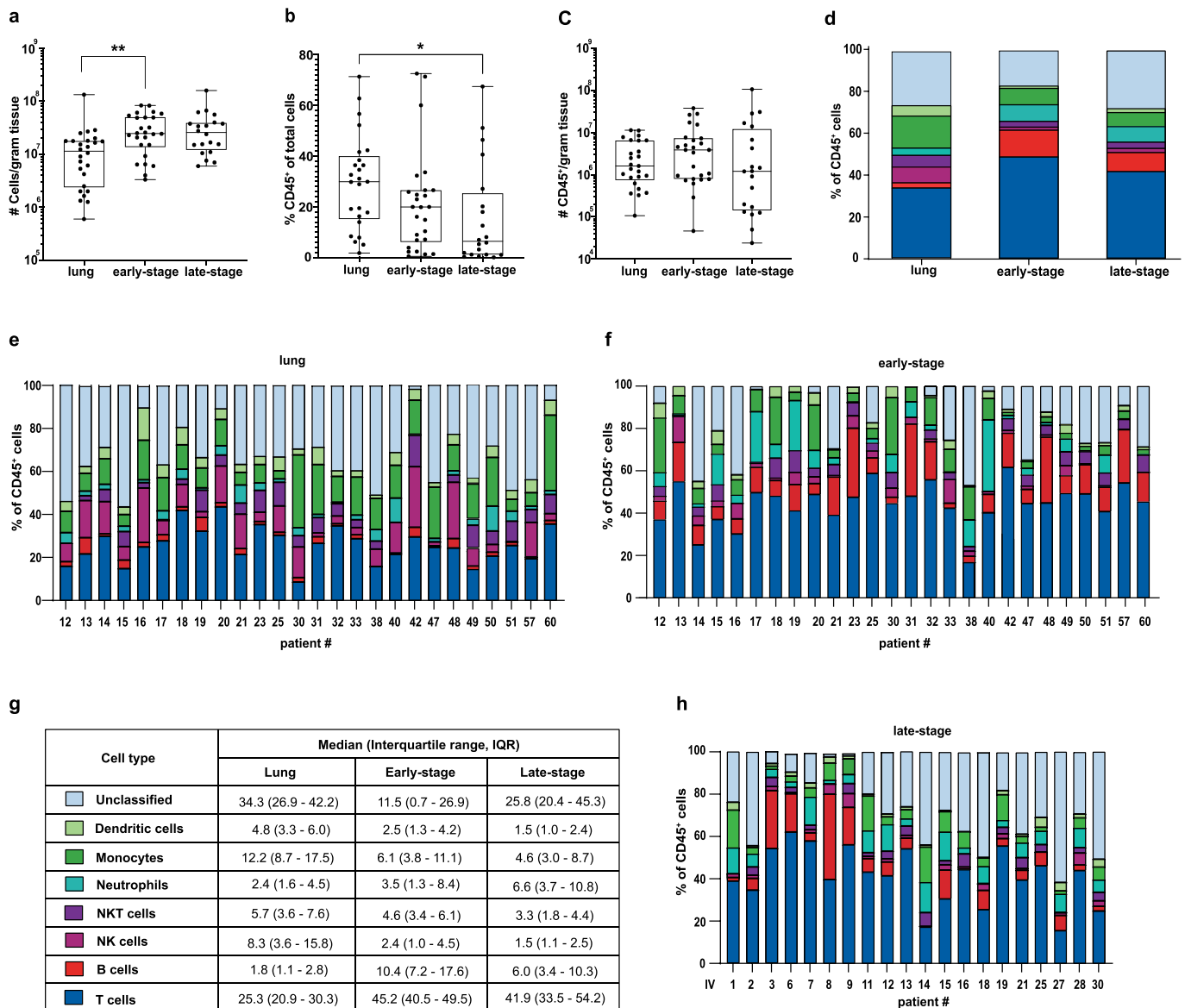
Figure 1. Increased T and B cell infiltrates in NSCLC tumor lesions with high inter-patient variability. (a) Cells per gram tissue obtained from lung tissue (left; *n* = 26), early-stage NSCLC tumor lesions (middle; *n* = 26) and late-stage NSCLC tumor lesions (right; *n* = 20) after digestion. (b, c) CD45+ immune infiltrates as (b) percentage of total number of cells, and (c) per gram tissue from indicated tissue digests. (d) Averaged percentages of various immune infiltrates of indicated tissue digests, immune cell types are colored according to cell type shown in panel G. (e-h) Composition of immune infiltrates in (e) lung tissue, (f) early-stage and (h) late-stage NSCLC tumor lesions from individual patients. (g) Percentages of immune infiltrates from E-H are presented as median with interquartile range. Statistical significance for lung and early-stage tumor digest was defined with paired t-test and for late-stage tumors compared to early-stage tumor and lung tissue with unpaired t-test. p-value *>0.05, **>0.005.

Cell type	Median (Interquartile range, IQR)		
	Lung	Early-stage	Late-stage
Unclassified	34.3 (26.9 - 42.2)	11.5 (0.7 - 26.9)	25.8 (20.4 - 45.3)
Dendritic cells	4.8 (3.3 - 6.0)	2.5 (1.3 - 4.2)	1.5 (1.0 - 2.4)
Monocytes	12.2 (8.7 - 17.5)	6.1 (3.8 - 11.1)	4.6 (3.0 - 8.7)
Neutrophils	2.4 (1.6 - 4.5)	3.5 (1.3 - 8.4)	6.6 (3.7 - 10.8)
NKT cells	5.7 (3.6 - 7.6)	4.6 (3.4 - 6.1)	3.3 (1.8 - 4.4)
NK cells	8.3 (3.6 - 15.8)	2.4 (1.0 - 4.5)	1.5 (1.1 - 2.5)
B cells	1.8 (1.1 - 2.8)	10.4 (7.2 - 17.6)	6.0 (3.4 - 10.3)
T cells	25.3 (20.9 - 30.3)	45.2 (40.5 - 49.5)	41.9 (33.5 - 54.2)

correlates with high B cell infiltrates in the tumor digest. High B cell infiltrates come with CD38+BCL6+ GC B cells, BCL6+IgD+ mantle zone B cells and BCL6+CXCR5+ follicular T helper cells, all of which are found in TLS.[43,44,49] Concomitant with these findings, we detected higher percentages of naïve T cells in tumor digests with high B cell infiltrates.

Previous reports showed that high B cell infiltrates, including the presence of TLS, are positive indicators for good response rates to checkpoint inhibitors.[23,25] Therefore, it may seem counterintuitive that high B cell infiltrates in the tumor digest negatively correlate with tumor-reactivity of expanded TIL products. We postulate that this divergence stems from the different starting point of these two therapeutic approaches.

The anti-tumoral effect of checkpoint inhibitors depends not only on re-activation of tumor-specific T cells infiltrating the tumor,[31,33,54,55] but also on the activation of newly generated tumor-specific T cell responses. The latter occurs in draining lymph nodes and in TLS,[56] ensuring a continuous recruitment of novel T cell clones during the treatment. The therapeutic success of checkpoint inhibition thus relies on dynamic changes of immune cell infiltrates and activity in the TME. Conversely, the generation of tumor-reactive TIL products from tumor lesions depends entirely on the status quo of T cell infiltrates at the time of tumor excision. To obtain tumor-reactive TIL products, the tumor lesion must already contain tumor-reactive TILs, which can be expanded and reset to potent effector T cells during the 4 weeks expansion protocol
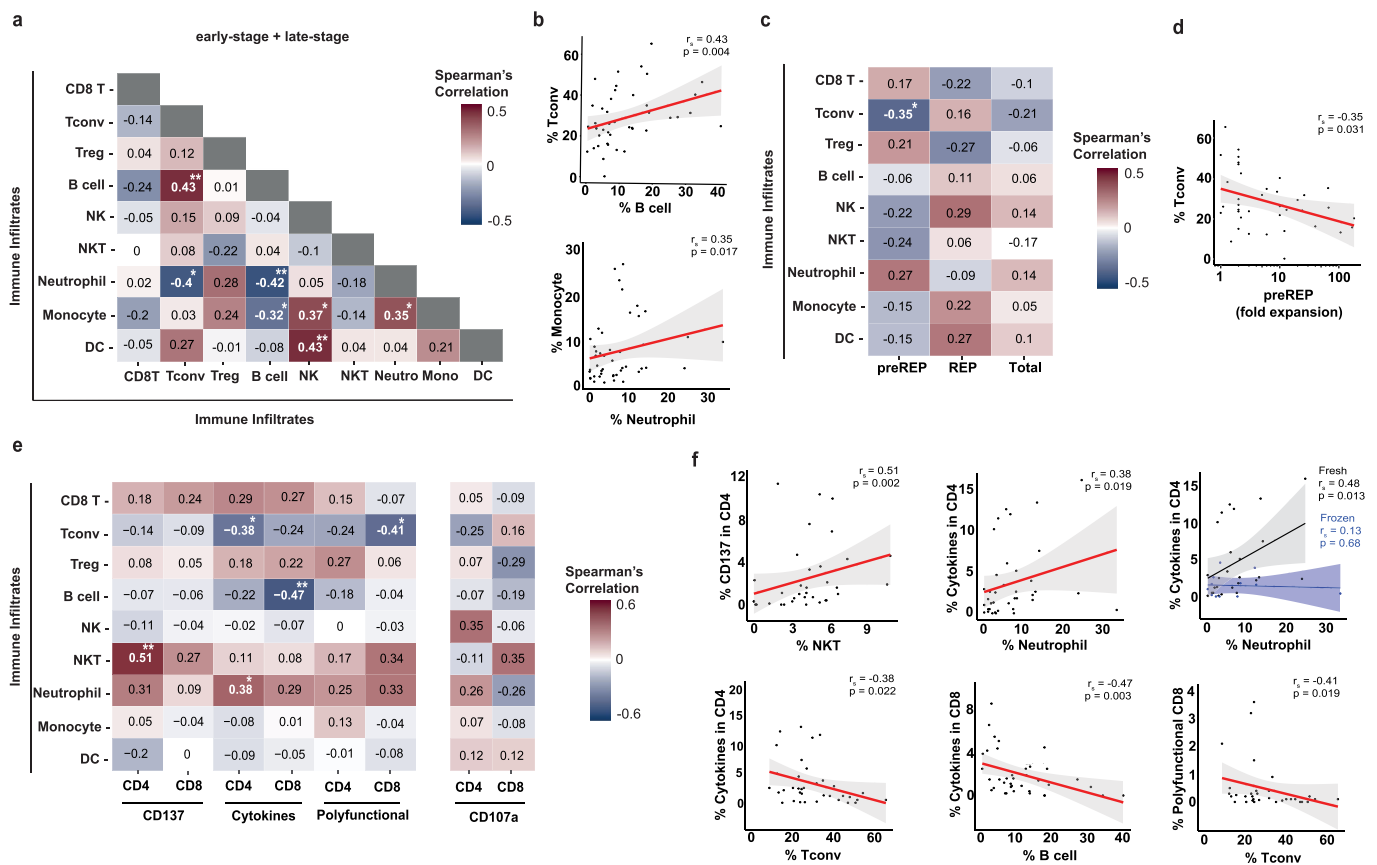
Figure 2. Tumor-specific immune infiltrates correlate with T cell functionality of expanded TIL products. (a) Correlation heatmap between different immune infiltrates of early- and late-stage NSCLC tumor lesions combined ($n = 46$). (b) Scatterplots show significant correlations between B cell infiltrate with conventional CD4$^+$ T cells, and monocyte infiltrate with neutrophils. (c) Correlation heatmap between the percentage of immune infiltrate subsets of early-stage and late-stage NSCLC tumor lesions combined with the expansion rate (fold change) of T cells during preREP (first 1-13 days), REP (second 1-13 days) and total expansion phase (preREP + REP). (d) The scatterplot shows the correlation between the percentage of conventional CD4$^+$ T cells with the preREP phase. (e) Correlation heatmap of indicated immune infiltrates of NSCLC tumor lesions ex vivo with anti-tumoral response of expanded TIL products, as defined by CD137 expression, production of at least one of the key cytokines (IFNγ, TNF, and/or IL-2), production of two or more cytokines (polyfunctional) for the entire cohort, and CD107α expression ($n = 29$) and by CD4$^+$ and CD8$^+$ T cells, after 6-7 h of co-culture with autologous tumor digest. (f) Scatterplots show significant correlations from panel (e) depicted for individual patients. The upper right scatterplot shows the division for patient samples with expansion starting from fresh material (black) or cryopreserved material (blue). All correlation heatmaps report Spearman's coefficient (r_s) and *$p < 0.05$, **$p < 0.005$. All scatterplots show the Spearman's coefficient (r_s) and p-value. The red line indicates the regression line of the correlation, and the gray area represents the confidence interval.

of the TIL cultures. The success of TIL therapy thus depends on available T cell clones within the tumor lesions at the starting point of expansion. It is thus tempting to speculate that whereas TLS support the activity of checkpoint inhibitors in the patients, a high prevalence of TLS-associated immune infiltrates, which increases the presence of naïve bystander T cells that still need to be primed,[41,43] rather hampers the effective outgrowth of tumor-reactive T cell during expansion. Probably, these naïve 'bystander' T cells outcompete the tumor-responsive TILs in number, and possibly in expansion capacity. Therefore, a pragmatic solution as B cell depletion before starting the expansion, will not do the trick to optimize the generation of tumor-responsive TIL products. Combined, our findings strongly suggest that the parameters defining the treatment success of checkpoint inhibitors versus TIL therapy differ. In line with this hypothesis, recent studies showed that patients that were refractory to checkpoint inhibitors can still benefit from TIL therapy.[7,15]

It is noteworthy that TLS in tumors can have different maturation statuses.[57] Only the presence of immature TLS correlated with improved progression free survival and overall survival in NSCLC patients.[58] This correlation fell short for tumors containing mature TILs with high numbers of antibody secreting B cells, Tfh cells and follicular-DCs.[58] Based on the limited number of samples available to validate the presence of BCL6$^+$ B cells and Tfh cells, we cannot draw any conclusions on mature or immature TLS present in the tumor lesions. The same accounts for the regulatory effect B cells theoretically can exert on TIL cultures, by secreting IL-10.[59] For future studies, it would be interesting to study the regulatory potential of B cells, for example to investigate if an increased B cell infiltrate in tumor lesions also indicates an increased IL-10 secreting B cell population. Nonetheless, in this cohort there was no correlation between B cell infiltrates and expansion potential of the TIL products (Figure 2(c)). Furthermore, it would be interesting to include the CXCL13-CXCR5 axis in future studies. One would speculate that, if indeed TLS are influencing the T cell state in the TME, and cause an influx of CXCR5$^+$ CD4$^+$ Tfh cells, there would also be an increase of CXCL13$^+$ CD8$^+$ T cells in the tumor, might explaining the lack of anti-tumor response from the TIL products.[60] In future studies, it would be of added value to include IHC or other spatial phenotype panels, to
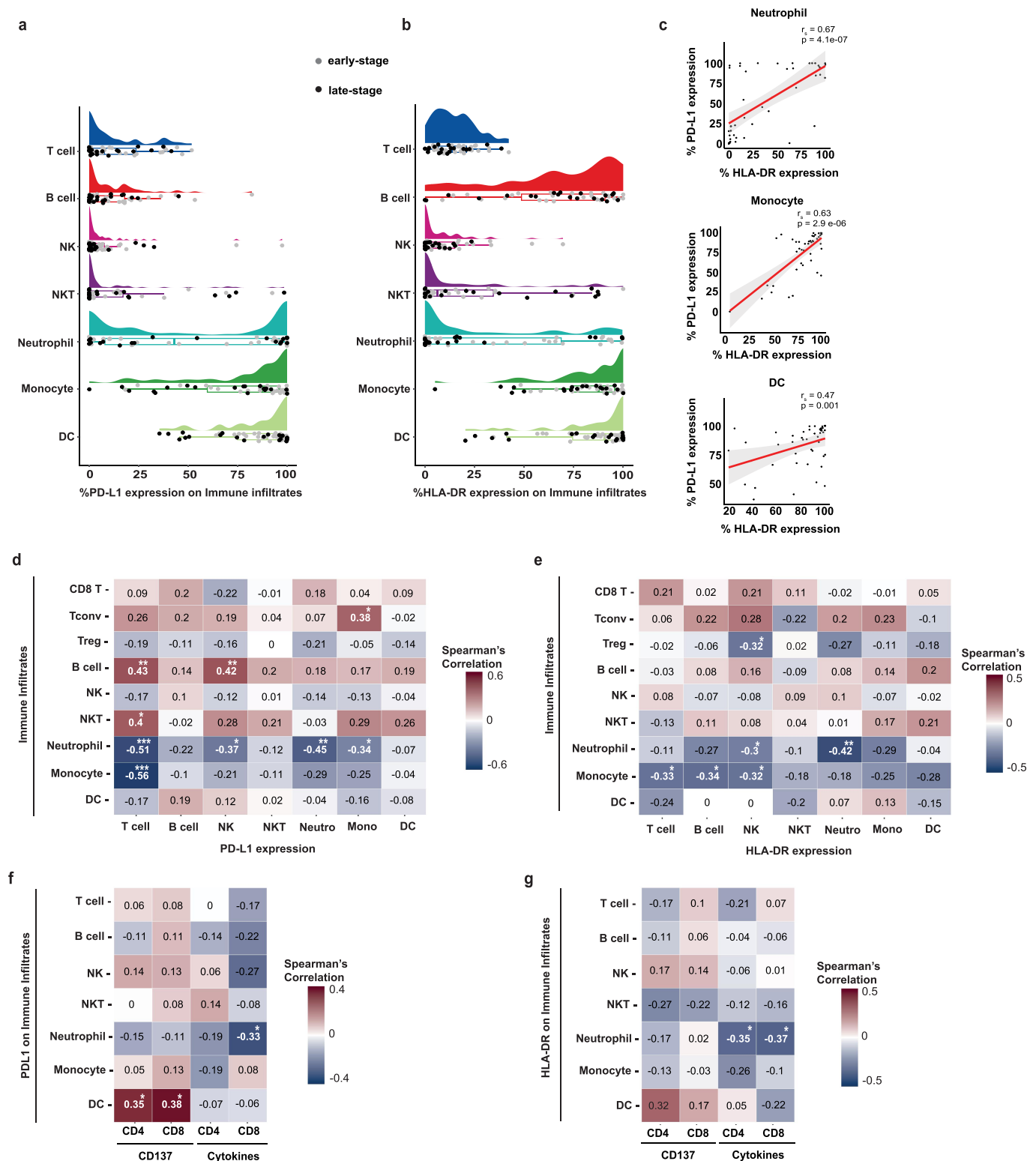
Figure 3. PD-L1 and HLA-DR expression on DCs and neutrophils correlate with T cell functionality. (a, b) Raincloud plots of (a) PD-L1 and (b) HLA-DR expression on different immune cell subsets of early-stage (gray dots) and late-stage (black dots) NSCLC tumors. Per cell type, a density plot (top) and boxplot with each dot corresponding to individual patients is shown. (c) Scatterplots show correlation between PD-L1 and HLA-DR expression on indicated cell types. (d, e) Correlation heatmaps of different immune cell infiltrates with the percentage of (d) PD-L1 expression and (e) HLA-DR expression on different immune infiltrates. (f, g) Correlation heatmaps of different immune cell infiltrates with the percentage of (f) PD-L1 expression and (g) HLA-DR expression with indicated anti-tumoral response of expanded TIL products upon 6 h of co-culture with autologous tumor digest. All correlation heatmaps report Spearman's coefficient (r_s) and *$p < 0.05$, **$p < 0.005$, ***$p < 0.0005$. All scatterplots show the Spearman's coefficient (r_s) and p-value. The red line indicates the regression line of the correlation, and the gray area represents the confidence interval.
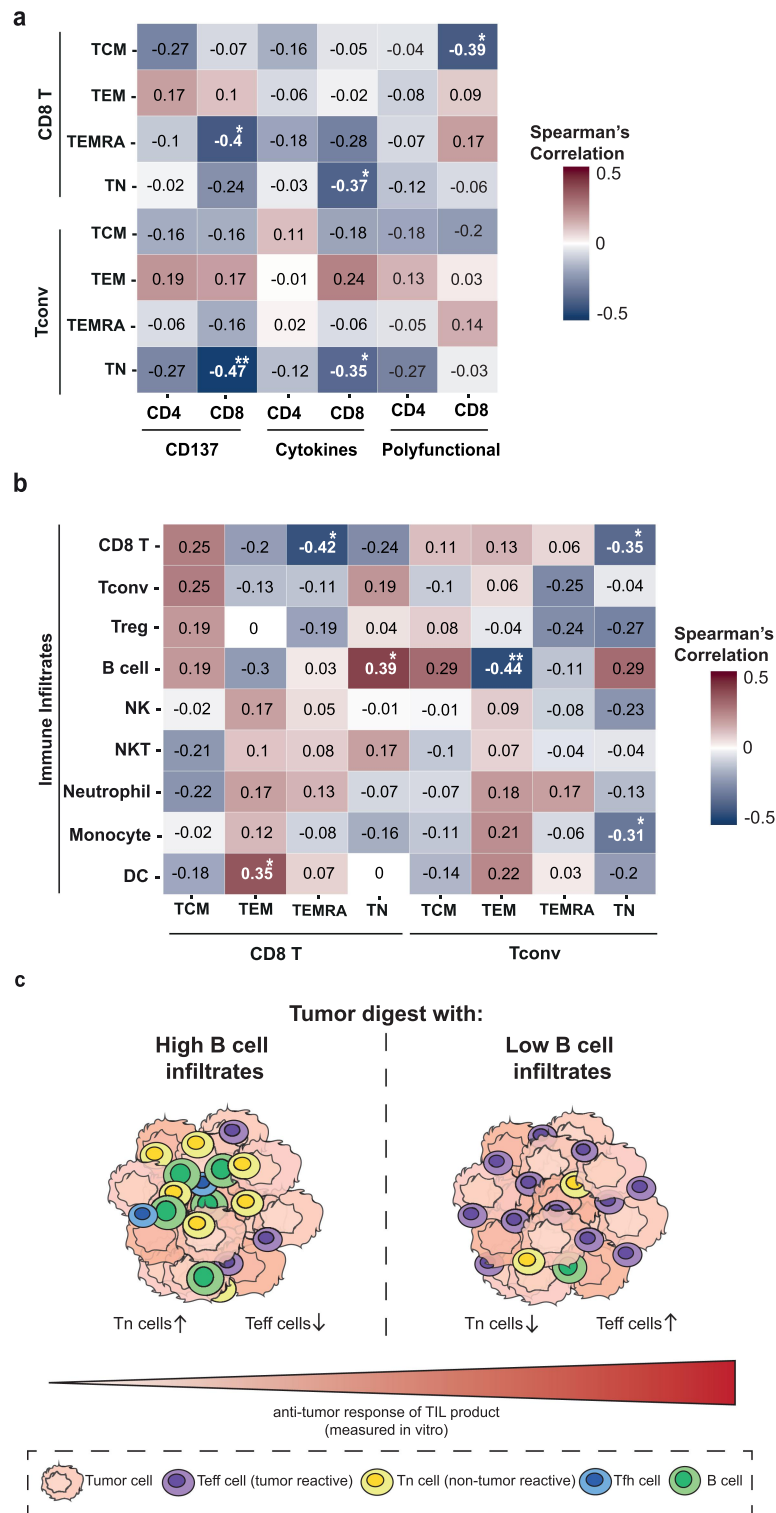
Figure 4. NSCLC lesions with high B cell infiltrates correlate with increased naïve T cell populations. (a) Correlation heatmap of T cell differentiation subsets in the tumor digest with indicated anti-tumoral response of expanded TIL products upon 6 h of co-culture with autologous tumor digest. (b) Correlation heatmap of different immune infiltrates with T cell differentiation subsets in the tumor digest. (c) Running hypothesis for the difference in tumor reactive TIL products from high and low B cell infiltrated NSCLC lesions. Teff: Effector T cell. Tn: naïve T cell. Tfh: follicular helper T cell. All correlation heatmaps report Spearman's coefficient (r_s) and *$p < 0.05$, **$p < 0.005$.

visualize the spatial composition within the tumor lesions used for TIL generation, with a focus on TLS-associated markers like BCL6, CXCR5 and CXCL13. With the digestion of the tumor pieces prior to the expansion protocol, spatial information is lost, which might even provide more information on the influence of the immune infiltrate.

We also observed other correlations of immune infiltrates with the tumor reactivity of TIL products. For instance, the
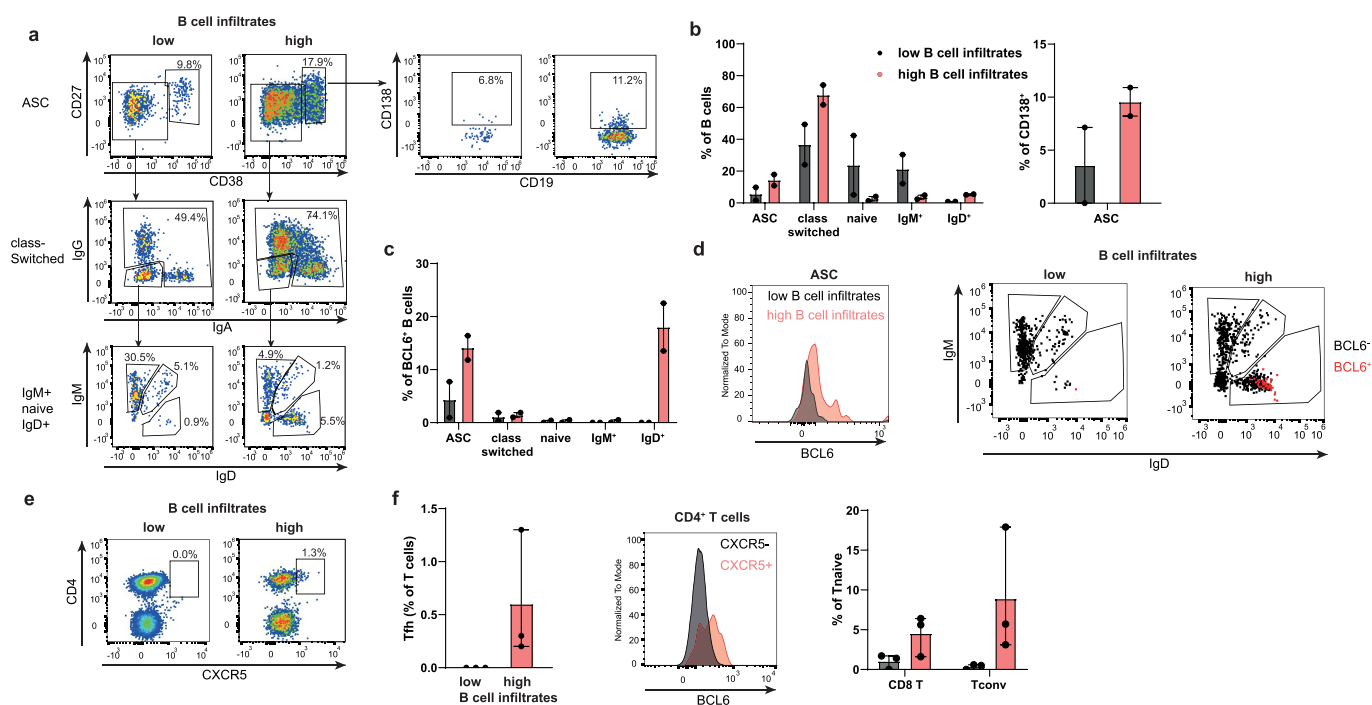
Figure 5. NSCLC lesions with high B cell infiltrates display tls-specific immune cell composition. (a) Representative gating on CD19^{+} B cells to identify CD27^{+} CD38^{+} antibody secreting cells (ASC), CD138^{+} CD27^{+} CD38^{+} B cells, IgA^{+} IgG^{+} CD27^{+} class-switched B cells, IgM^{+} IgD^{+} naïve B cells, and IgM^{+} B, or IgD^{+} B cells. (b) Compiled data of patient #30 and #IV-14 with low B cell infiltrates, and patient #31 and #42 with high B cell infiltrates and (c) percentage of BCL6 expression on indicated B cell subsets. (d) Left panel: BCL6 expression of ASC B cells derived from NSCLC lesions with low (black) or high (red) B cell infiltration. Right panel: Representative flow cytometry analysis of BCL6^{+} expression on IgD^{+} B cells. (e) Representative gating of CXCR5^{+} on CD4^{+}T cells. (f) Left panel: percentage of BCL6 expression on Tfh from patient #30, #IV-14 and #IV-16 (low B cell infiltration) and patient #31, #42 and #IV-15 (high B cell infiltration). Middle panel: representative BCL6 staining of tumor-infiltrating Tfh. Right panel: percentage of naïve T cells present in indicated tumor lesions. Bar graphs depict mean with range.

presence of neutrophils positively correlated with TIL functionality. Interestingly, this positive correlation primarily originated from neutrophils that lacked the expression of PD-L1 or HLA-DR. PD-L1 expression on neutrophils has been shown to block T cell activation and function[61] and correlates with poor outcome of hepatocellular carcinoma and gastric cancer patients.[62,63] Also in NSCLC, neutrophils are present in high numbers in the tumor lesions, and define the treatment outcome to immunotherapy,[23,28,64] as neutrophils are considered a negative prognostic factor for NSCLC patients treated with the checkpoint inhibitors.[23,28,65,66] Interestingly, we show here that high percentages of neutrophil infiltrates rather positively correlate with the tumor-reactivity in TIL products. This, however, only holds true when neutrophils express low levels of PD-L1 and HLA-DR. Furthermore, this feature is lost after neutrophil depletion before the start of expansion, due to the usage of cryo-preserved tumor digest (Figure 2(f)). This could indicate that neutrophils actively prime the T cells during the culture and therefore contribute to tumor-reactive TIL products. It would be interesting to further decipher the nature and heterogeneity of neutrophils within the tumor lesions. However, because neutrophils can only be phenotyped and further studied from freshly digested tumor lesions,[67] we could not follow up on this observation. Nevertheless, measuring the overall activation status of neutrophils may provide clues to define under which circumstances neutrophils are immunosuppressive, and if or how they are interacting with the T cells during the culture.

In conclusion, we show here that the efficacy of generating tumor-reactive TIL products correlates with the immune cell composition of the obtained tumor lesion. The role of immune composition substantially differs from what is required for patients to respond to checkpoint inhibition. Therefore, we propose that defining the composition of immune infiltrates may help define whether a patient is more likely to respond to checkpoint inhibition, or to TIL therapy.

Materials and methods

Tumor sample collection

Tumor samples were collected between April 2016 and November 2020. From early-stage patients, tissue from tumor lesions and healthy distal lung tissue was obtained (n = 30). From late-stage patients, tissue from metastatic tumor lesions were collected (n = 20). All tumor and tissue samples were measured in length at the pathology department. Four early-stage patients were excluded from the downstream analysis due to technical errors, resulting in a cohort of 26 early-stage NSCLC patients and 20 late-stage NSCLC patients. 11 early-stage and 18 late-stage patients had been included in previous reports[12,14] (Table 1 and 2). The study was performed according to the Declaration of Helsinki (seventh revision, 2013), with consent of the Institutional Review Board of the Netherlands Cancer Institute/Antoni van Leeuwenhoek

Hospital (NKI-AvL), Amsterdam, the Netherlands. Tumor and lung tissue was obtained and processed within 4 hours after surgery.

Tissue digestion

All samples were weighed prior to digestion. Tissue digestion was performed as previously described.[12,14] Briefly, freshly isolated tumor or lung tissue was finely chopped and enzymatically digested for 45 min at 37°C with RPMI (Gibco) containing 30 IU/ml collagenase IV (Worthington), 12,5 µg/ml DNAse (Roche), and 1% FBS (Bodego, Bodinco BV) to obtain a single cell suspension. Live and dead cells were manually counted with tryphan blue solution (Sigma) on a hemocytometer. Approximately 1×10^6 cells were used per antibody staining mix for flow cytometry analysis. The remaining digest was used for TIL expansion cultures, or cryo-preserved until further use.

TIL expansion

$1\text{-}3 \times 10^6$ cells were cultured in 24-well plates at 37°C and 5% CO2 in 20/80 T-cell mixed media (Miltenyi) containing 5% human serum (HS) (Sanquin), 5% FBS, 50 µg/ml gentamycin, 1.25 µg/ml fungizone, and 6000 IU human recombinant (hr) IL-2 (Proleukin, Novartis) for 10–13 days (pre-Rapid Expansion Phase; pre-REP). Cells were cultured for another 10–13 days (REP) with irradiated PBMCs pooled from 15 healthy blood donors, 30 ng/ml anti-CD3 antibody (OKT-3) (Miltenyi Biotec) and 3000 IU/ml hrIL-2 as previously reported.[12] Expanded TILs were used immediately for analysis, or cryo-preserved in RPMI medium 1640 containing 10% Dimethyl Sulfoxide (DMSO) (Corning) and 40% FBS until further use.

T cell activation

Expanded TILs (REP) were counted with tryphan blue staining. To allow for detection of CD4 and CD8 expression after activation, cells were pre-stained with anti-CD4 and anti-CD8 for 30 min at 4°C in MACS buffer (PBS supplemented with 2% FBS and 2 mM EDTA) and anti-CD107α was added at the start of the co-culture. Cells were washed once with MACS buffer and taken up in fresh 20/80 T cell mixed media. 1×10^5 TILs were co-cultured with 2×10^5 autologous tumor digest for 6–7 hours at 37°C. After 1 h, 1× Brefeldin A (Invitrogen), Monensin (Invitrogen) and anti-CD107α was added. As controls, expanded TILs were stimulated with 10 ng/ml phorbol myristate acetate (PMA) and 1 µg/ml ionomycin for 6-7 h, or cultured with T cell mixed medium alone.

Flow cytometry acquisition and analysis

Staining protocols for freshly digested tumor material or expanded TILs was previously described.[12,14] For detailed information about antibodies, see Table 3. Cells were washed twice with MACS buffer before staining. Live/dead fixable near-IR APC-Cy7 dye (Invitrogen) was included in surface staining mix for dead cell exclusion. Freshly digested single cell suspensions from tumor and lung tissue were stained with CD1a, anti-CD3, anti-CD11b, anti-CD11c, anti-CD14, anti-CD15, anti-CD16, anti-CD19, anti-CD20, anti-CD33, anti-CD45, anti-CD274, and anti-HLA-DR. For T cell differentiation analysis, single cell suspensions from digested tissue were stained with anti-CD3, anti-CD4, anti-CD8, anti-CD25, anti-CD27, anti-CD45RA, anti-CD127. Intracellular staining with anti-CD68 (freshly digested tumor lesions) and anti-Foxp3 (T cell differentiation) was performed after fixation for 30 min with Perm/Fix Foxp3 staining kit (ebioscience), according to the manufacturer's protocol.

After T cell activation, cells were washed twice with MACS buffer and stained with anti-CD3. Live/dead fixable near-IR APC-Cy7 dye (Invitrogen) was included for dead cell exclusion. Cells were washed twice with MACS buffer and fixed for 30 min with Perm/Fix Foxp3 staining kit (according to the manufacturer's protocol) and stained with anti-CD137, anti-IL2, anti-IFNγ, and anti-TNF for 30 min at 4°C.

Cells were washed once with 1× Perm/Wash (ebioscience), taken up in MACS buffer and passed through a 70 µm single-cell filter prior to flow cytometric analysis on Symphony A5 (BD Biosciences). To ensure reproducibility, flow cytometry settings were defined for each patient with single antibody staining, and a standardized PBMC sample pooled from 4 healthy donors that was cryopreserved before the start of the study and used throughout.

Phenotypic analysis of tumor-infiltrating B cells and CD4$^+$ T cells was performed on cryopreserved tumor digest patients with low B cell infiltrates (#30, #IV-14, #IV-16), patients with high B cell infiltrates (#31, #42, #IV-15). Defrosted cells were incubated for 1 hour at 37°C in RPMI at 2×10^6 cells/ml containing 5% HS, 5% FBS, 50 µg/ml gentamycin, 1.25 µg/ml fungizone and 50 IU hrIL-2 (culture medium; CM), and then stained in MACS buffer for 30 min at 4°C with anti-CD3, anti-CD4, anti-CD11c, anti-CD19, anti-CD21, anti-CD24, anti-CD27, anti-CD38, anti-CD138, anti-IgA, anti-IgD, anti-IgG and anti-IgM, see detailed information in Table 3. Live/dead fixable near-IR APC-Cy7 dye (Invitrogen) was included for dead cell exclusion. Cells were washed twice with MACS buffer and fixed for 30 min with Perm/Fix Foxp3 staining kit and stained with anti-CXCR5 and anti-BCL6[68] for 30 min at 4°C, according to manufacturer's protocol. Cells were washed once with Perm/Wash, taken up in MACS buffer and passed through a 70 µm single-cell filter prior to flow cytometry analysis on ID7000 Spectral Cell Analyzer (Sony Biotechnologies). Data analysis was performed with FlowJo Star 10.7.1 (BD).

Gating in R

For flow cytometry measurements of T cell subsets and T cell differentiation status from tumors that had not been reported previously (Table 2), and PD-L1 and HLA-DR expression on immune infiltrates were analyzed in R (version 4.1.1).[69] FCS files were exported from the Symphony A5 (BD Biosciences) flow cytometer and imported into the R environment using flowCore package (version 2.4), and then cleaned with flowAI package (version 1.22.0).[70,71] Cleaned FCS files were compensated using CytoExploreR package (version 1.1.0).[72] Manual and automated gates with OpenCyto package (version 2.4)[73] were used to gate for different T cell subsets and T cell

differentiation states (supplemental figure S2A and S4A), as well as for PD-L1 and HLA-DR expression on immune infiltrates (supplemental figure S3A). The resulting gates were visualized with ggcyto package (version 1.20.0).[74]

Data processing

To define the overall lymphoid and myeloid infiltrates from tumor lesions and lung tissue, FCS files from FACSDiva were exported, compensated and pre-gated in FlowJo Star v10.7.1 to remove debris, doublets, dead cells, and to enrich for $CD45^+$ live cells. Pre-gated FCS files were exported from FlowJo and pre-processed in a multistep analysis with an in-house developed R pipeline (https://github.com/NandhiniKanagasabesan/NSCLC_Project). First, FCS files were imported into the R environment, and expression values of selected markers were extracted from each FCS file with flowCore package (version 2.4) (supplemental figure S1B).[75] Batch correction for all patient combined was performed as follow: 1) The marker expression values were transformed using hyperbolic arcsine transformation, which linearizes near-zero values and logarithmically transforms higher positive and negative values with rrscale package (version 1)[70,76] and 2) Transformed data were then median-centered and scaled.[70]

Clustering in CytoTree

Pre-processed FCS files were clustered and visualized with CytoTree package in R (version 1.3).[77] For UMAPs, the expression values from each pre-processed FCS file were merged using the ceil method. Pre-processed FCS file with more than 50k cells, with sub-sampled at random 50k cells (without replacement); otherwise, all data was used and aggregated to allow for downstream application. The expression matrix and metadata (patient ID) were combined to build a CYT object, on which unsupervised clustering was performed with self-organizing maps (SOM), resulting in 25 clusters. Clusters were processed by dimensionality reduction (UMAP). Tree-shaped trajectories were built using minimum spanning tree (MST) approach. With heatmap visualization and tree plot, clusters were assigned to meta clusters (immune cell populations) that were identified by comparing the expression of markers (supplemental figure S1B). Clusters of immune cell populations were visualized on a 2-dimensional UMAP plot.

Statistical analysis and data visualization

The percentage of live immune infiltration was calculated with CytoTree package in R. The difference between lung and early-stage lesions was calculated with paired Student t-test, and between early stage and late-stage lesions with unpaired Student t-test. Correlation of immune infiltrates with immune infiltrates, TIL expansion and with tumor reactivity was calculated using Spearman's Rank correlation with Hmisc R package (version 4.7.1).[78] The correlation was considered statistically significant when p-value <0.05.

Plots, correlation heatmaps and raincloud plots were generated with GraphPad Prism (Dotmatics, version 9.1.1), Cytotree (version 1.3), ggplot2 (version 3.4.2),[77,79] and ggdist (version 3.3)[80] packages in R.

ORCID

Monika C. Wolkers (iD) http://orcid.org/0000-0003-3242-1363

Authors' contributions

MvL, RdG, SC and MW designed the project. AG, MvL, RdG and SC performed the practical work, SC and NK performed data analysis. SC and MW wrote the manuscript. All authors provided input on the manuscript. MW supervised the study.

Data availability statement

The authors confirm that the data supporting the findings of this study are available within the article and its supplementary materials.

References

1. Rosenberg SA, Restifo NP. Adoptive cell transfer as personalized immunotherapy for human cancer. Sci. 2015;348(6230):62–68. doi:10.1126/science.aaa4967.
2. Rosenberg SA, Dudley ME. Adoptive cell therapy for the treatment of patients with metastatic melanoma. Curr Opin Immunol. 2009;21(2):233. doi:10.1016/j.coi.2009.03.002.
3. Dudley ME, Gross CA, Langhan MM, Garcia MR, Sherry RM, Yang JC, Phan GQ, Kammula US, Hughes MS, Citrin DE, et al. CD8+ enriched "young" tumor infiltrating lymphocytes can mediate regression of metastatic melanoma. Clin Cancer Res. 2010;16 (24):6122. doi:10.1158/1078-0432.CCR-10-1297.
4. Besser MJ, Shapira-Frommer R, Treves AJ, Zippel D, Itzhaki O, Hershkovitz L, Levy D, Kubi A, Hovav E, Chermoshniuk N, et al.

Clinical responses in a phase II study using adoptive transfer of short-term cultured tumor infiltration lymphocytes in metastatic melanoma patients. Clin Cancer Res. 2010;16(9):2646–2655. doi:10.1158/1078-0432.CCR-10-0041.

5. Radvanyi LG, Bernatchez C, Zhang M, Fox PS, Miller P, Chacon J, Wu R, Lizee G, Mahoney S, Alvarado G, et al. Specific lymphocyte subsets predict response to adoptive cell therapy using expanded autologous tumor-infiltrating lymphocytes in metastatic melanoma patients. Clin Cancer Res. 2012;18(24):6758. doi:10.1158/1078-0432.CCR-12-1177.

6. Berg JHVD, Heemskerk B, van Rooij N, Gomez-Eerland R, Michels S, van Zon M, de Boer R, Bakker NAM, Jorritsma-Smit A, van Buuren MM, et al. Tumor infiltrating lymphocytes (TIL) therapy in metastatic melanoma: boosting of neoantigen-specific T cell reactivity and long-term follow-up. J Immunother Cancer. 2020;8(2):e000848. doi:10.1136/jitc-2020-000848.

7. Rohaan MW, Borch TH, van den Berg JH, Met Ö, Kessels R, Geukes Foppen MH, Stoltenborg Granhøj J, Nuijen B, Nijenhuis C, Jedema I, et al. Tumor-infiltrating lymphocyte therapy or ipilimumab in advanced melanoma. N Engl J Med. 2022;387 (23):2113–2125. doi:10.1056/NEJMoa2210233.

8. Besser MJ, Shapira-Frommer R, Itzhaki O, Treves AJ, Zippel DB, Levy D, Kubi A, Shoshani N, Zikich D, Ohayon Y, et al. Adoptive transfer of tumor-infiltrating lymphocytes in patients with metastatic melanoma: intent-to-treat analysis and efficacy after failure to prior immunotherapies. Clin Cancer Res. 2013;19 (17):4792–4800. doi:10.1158/1078-0432.CCR-13-0380.

9. Poch M, Hall M, Joerger A, Kodumudi K, Beatty M, Innamarato PP, Bunch BL, Fishman MN, Zhang J, Sexton WJ, et al. Expansion of tumor infiltrating lymphocytes (TIL) from bladder cancer. Oncoimmunol. 2018;7(9):e1476816. doi:10.1080/2162402X.2018.1476816.

10. Pedersen M, Westergaard MCW, Milne K, Nielsen M, Borch TH, Poulsen LG, Hendel HW, Kennedy M, Briggs G, Ledoux S, et al. Adoptive cell therapy with tumor-infiltrating lymphocytes in patients with metastatic ovarian cancer: a pilot study. Oncoimmunol. 2018;7 (12):e1502905. doi:10.1080/2162402X.2018.1502905.

11. van Asten SD, de Groot R, van Loenen MM, Castenmiller SM, de Jong J, Monkhorst K, Haanen JBAG, Amsen D, Bex A, Spaapen RM, et al. T cells expanded from renal cell carcinoma display tumor-specific CD137 expression but lack significant ifn-γ, tnf-α or IL-2 production. OncoImmunol. 2021;10(1). doi:10.1080/2162402X.2020.1860482.

12. De Groot R, Van Loenen MM, Guislain A, Nicolet BP, Freen-Van Heeren JJ, Verhagen OJHM, Van Den Heuvel MM, De Jong J, Burger P, Van Der Schoot CE, et al. Polyfunctional tumor-reactive T cells are effectively expanded from non-small cell lung cancers, and correlate with an immune-engaged T cell profile. Oncoimmunol. 2019;8(11):e1648170. doi:10.1080/2162402X.2019.1648170.

13. Ben-Avi R, Farhi R, Ben-Nun A, Gorodner M, Greenberg E, Markel G, Schachter J, Itzhaki O, Besser MJ. Establishment of adoptive cell therapy with tumor infiltrating lymphocytes for non-small cell lung cancer patients. Cancer Immunol Immunother. 2018;67 (8):1221–1230. doi:10.1007/s00262-018-2174-4.

14. Castenmiller SM, de Groot R, Guislain A, Monkhorst K, Hartemink KJ, Veenhof AAFA, Smit EF, Haanen JBAG, Wolkers MC. Effective generation of tumor-infiltrating lymphocyte products from metastatic non-small-cell lung cancer (NSCLC) lesions irrespective of location and previous treatments. Immuno-Oncol Technol. 2022;15:100090. doi:10.1016/j.iotech.2022.100090.

15. Creelan BC, Wang C, Teer JK, Toloza EM, Yao J, Kim S, Landin AM, Mullinax JE, Saller JJ, Saltos AN, et al. Tumor-infiltrating lymphocyte treatment for anti-PD-1-resistant metastatic lung cancer: a phase 1 trial. Nat Med. 2021;27 (8):1410–1418. doi:10.1038/s41591-021-01462-y.

16. Zhao Y, Deng J, Rao S, Guo S, Shen J, Du F, Wu X, Chen Y, Li M, Chen M, et al. Tumor infiltrating lymphocyte (TIL) therapy for solid tumor treatment: progressions and challenges. Cancers (Basel). 2022;14(17):4160. doi:10.3390/cancers14174160.

17. Coukos G. TIL therapy entering the mainstream. N Engl J Med. 2022;387(23):2185–2186. doi:10.1056/NEJMe2214655.

18. Robert C, Schachter J, Long GV, Arance A, Grob JJ, Mortier L, Daud A, Carlino MS, McNeil C, Lotem M, et al. Pembrolizumab versus ipilimumab in advanced melanoma. N Engl J Med. 2015;372 (26):2521–2532. doi:10.1056/NEJMoa1503093.

19. Reck M, Rodríguez-Abreu D, Robinson AG, Hui R, Csőszi T, Fülöp A, Gottfried M, Peled N, Tafreshi A, Cuffe S, et al. Pembrolizumab versus chemotherapy for PD-L1–positive non–small-cell lung cancer. N Engl J Med. 2016;375(19):1823–1833. doi:10.1056/NEJMoa1606774.

20. Smit EF, de Langen AJ. Pembrolizumab for all PD-L1-positive NSCLC. The Lancet. 2019;393(10183):1776–1778. doi:10.1016/S0140-6736(18)32559-5.

21. Frisone D, Friedlaender A, Addeo A, Tsantoulis P. The landscape of immunotherapy resistance in NSCLC. Front Oncol. 2022;12. doi:10.3389/fonc.2022.817548.

22. Hong JJ, Rosenberg SA, Dudley ME, Yang JC, White DE, Butman JA, Sherry RM. Successful treatment of melanoma brain metastases with adoptive cell therapy. Clin Cancer Res. 2010;16 (19):4892–4898. doi:10.1158/1078-0432.CCR-10-1507.

23. Salcher S, Sturm G, Horvath L, Untergasser G, Kuempers C, Fotakis G, Panizzolo E, Martowicz A, Trebo M, Pall G, et al. High-resolution single-cell atlas reveals diversity and plasticity of tissue-resident neutrophils in non-small cell lung cancer. Cancer Cell. 2022;40(12):1503. doi:10.1016/j.ccell.2022.10.008.

24. Backman M, Strell C, Lindberg A, Mattsson JSM, Elfving H, Brunnström H, O'Reilly A, Bosic M, Gulyas M, Isaksson J, et al. Spatial immunophenotyping of the tumour microenvironment in non–small cell lung cancer. Eur J Cancer. 2023;185:40–52. doi:10.1016/j.ejca.2023.02.012.

25. Germain C, Gnjatic S, Tamzalit F, Knockaert S, Remark R, Goc J, Lepelley A, Becht E, Katsahian S, Bizouard G, et al. Presence of B cells in tertiary lymphoid structures is associated with a protective immunity in patients with lung cancer. Am J Respir Crit Care Med. 2014;189(7):832–844. doi:10.1164/rccm.201309-1611OC.

26. Krishna S, Lowery FJ, Copeland AR, Bahadiroglu E, Mukherjee R, Jia L, Anibal JT, Sachs A, Adebola SO, Gurusamy D, et al. Stem-like CD8 T cells mediate response of adoptive cell immunotherapy against human cancer. Science. 2020;370(6522):1328–1334. doi:10.1126/science.abb9847.

27. Barras D, Ghisoni E, Chiffelle J, Orcurto A, Dagher J, Fahr N, Benedetti F, Crespo I, Zimmermann S, Duran R, et al. Tumor microenvironment cellular crosstalk predicts response to adoptive TIL therapy in melanoma. bioRxiv. 2022; doi:10.1101/2022.12.23.519261.

28. Kargl J, Busch SE, Yang GHY, Kim K-H, Hanke ML, Metz HE, Hubbard JJ, Lee SM, Madtes DK, McIntosh MW, et al. Neutrophils dominate the immune cell composition in non-small cell lung cancer. Nat Commun. 2017;8(1). doi:10.1038/ncomms14381.

29. Stankovic B, Bjørhovde HAK, Skarshaug R, Aamodt H, Frafjord A, Müller E, Hammarström C, Beraki K, Bækkevold ES, Woldbæk PR, et al. Immune cell composition in human non-small cell lung cancer. Front Immunol. 2019;9:3101. doi:10.3389/fimmu.2018.03101.

30. Kim HR, Ha S-J, Hong MH, Heo SJ, Koh YW, Choi EC, Kim EK, Pyo KH, Jung I, Seo D, et al. PD-L1 expression on immune cells, but not on tumor cells, is a favorable prognostic factor for head and neck cancer patients. Sci Rep. 2016;6(1):36956. doi:10.1038/srep36956.

31. Kim Y, Wen X, Cho NY, Kang GH. Intratumoral immune cells expressing PD-1/PD-L1 and their prognostic implications in cancer: a meta-analysis. Int J Biol Markers. 2018;33(4):467–474. doi:10.1177/1724600818770941.

32. Mei J, Jiang G, Chen Y, Xu Y, Wan Y, Chen R, Liu F, Mao W, Zheng M, Xu J, et al. HLA class II molecule HLA-DRA identifies immuno-hot tumors and predicts the therapeutic response to anti-PD-1 immunotherapy in NSCLC. BMC Cancer. 2022;22 (1):738. doi:10.1186/s12885-022-09840-6.

33. Mispelbaum R, Hattenhauer ST, Held SAE, Brossart P, Heine A. Baseline immune signature score of tregs × HLA-DR+CD4+ T cells × PD1+CD8+ T cells predicts outcome to immunotherapy in cancer patients. Front Immunol. 2022;13. doi:10.3389/fimmu.2022.1054161.

34. Johnson AM, Boland JM, Wrobel J, Klezcko EK, Weiser-Evans M, Hopp K, Heasley L, Clambey ET, Jordan K, Nemenoff RA, et al. Cancer cell-specific major histocompatibility complex II expression as a determinant of the immune infiltrate organization and function in the NSCLC tumor microenvironment. J Thorac Oncol. 2021;16(10):1694–1704. doi:10.1016/j.jtho.2021.05.004.

35. Diskin B, Adam S, Cassini MF, Sanchez G, Liria M, Aykut B, Buttar C, Li E, Sundberg B, Salas RD, et al. PD-L1 engagement on T cells promotes self-tolerance and suppression of neighboring macrophages and effector T cells in cancer. Nat Immunol. 2020;21 (4):442–454. doi:10.1038/s41590-020-0620-x.

36. Sierra JM, Secchiari F, Nuñez SY, Iraolagoitia XLR, Ziblat A, Friedrich AD, Regge MV, Santilli MC, Torres NI, Gantov M, et al. Tumor-experienced human NK cells express high levels of PD-L1 and inhibit CD8+ T cell proliferation. Front Immunol. 2021;12:745939. doi:10.3389/fimmu.2021.745939.

37. Yu H, Boyle TA, Zhou C, Rimm DL, Hirsch FR. PD-L1 expression in lung cancer. J Thorac Oncol. 2016;11(7):964. doi:10.1016/j.jtho.2016.04.014.

38. Ahmadzadeh M, Johnson LA, Heemskerk B, Wunderlich JR, Dudley ME, White DE, Rosenberg SA. Tumor antigen–specific CD8 T cells infiltrating the tumor express high levels of PD-1 and are functionally impaired. Blood. 2009;114(8):1537. doi:10.1182/blood-2008-12-195792.

39. Coughlin CM, Fleming MD, Carroll RG, Pawel BR, Hogarty MD, Shan X, Vance BA, Cohen JN, Jairaj S, Lord EM, et al. Immunosurveillance and survivin-specific T-cell immunity in children with high-risk neuroblastoma. J Clin Oncol. 2006;24 (36):5725–5734. doi:10.1200/JCO.2005.05.3314.

40. Ghorani E, Reading JL, Henry JY, Massy MRD, Rosenthal R, Turati V, Joshi K, Furness AJS, Ben Aissa A, Saini SK, et al. The T cell differentiation landscape is shaped by tumour mutations in lung cancer. Nat Cancer. 2020;1(5):546–561. doi:10.1038/s43018-020-0066-y.

41. Yu P, Lee Y, Liu W, Chin RK, Wang J, Wang Y, Schietinger A, Philip M, Schreiber H, Fu Y-X, et al. Priming of naive T cells inside tumors leads to eradication of established tumors. Nat Immunol. 2004;5(2):141–149. doi:10.1038/ni1029.

42. Sakai Y, Hoshino H, Kitazawa R, Kobayashi M. High endothelial venule-like vessels and lymphocyte recruitment in testicular seminoma. Androl. 2014;2(2):282–289. doi:10.1111/j.2047-2927.2014.00192.x.

43. Domblides C, Rochefort J, Riffard C, Panouillot M, Lescaille G, Teillaud J-L, Mateo V, Dieu-Nosjean M-C. Tumor-associated tertiary lymphoid structures: from basic and clinical knowledge to therapeutic manipulation. Front Immunol. 2021;12:698604. doi:10.3389/fimmu.2021.698604.

44. Cattoretti G, Shaknovich R, Smith PM, Jäck H-M, Murty VV, Alobeid B. Stages of germinal center transit are defined by B cell transcription factor coexpression and relative abundance. J Immunol. 2006;177(10):6930–6939. doi:10.4049/jimmunol.177.10.6930.

45. Ioannidou K, Ndiaye D-R, Noto A, Fenwick C, Fortis SP, Pantaleo G, Petrovas C, de Leval L. In situ characterization of follicular helper CD4 T cells using multiplexed imaging. Front Immunol. 2021;11:607626. doi:10.3389/fimmu.2020.607626.

46. Apostolidis SA, Kakara M, Painter MM, Goel RR, Mathew D, Lenzi K, Rezk A, Patterson KR, Espinoza DA, Kadri JC, et al. Cellular and humoral immune responses following SARS-CoV-2 mRNA vaccination in patients with multiple sclerosis on anti-CD20 therapy. Nat Med. 2021;27(11):1990–2001. doi:10.1038/s41591-021-01507-2.

47. Singh D, Ganesan AP, Panwar B, Eschweiler S, Hanley CJ, Madrigal A, Ramírez-Suástegui C, Wang A, Clarke J, Wood O, et al. CD4+ follicular helper-like T cells are key players in anti-tumor immunity. bioRxiv. 2020; doi:10.1101/2020.01.08.898346.

48. Niogret J, Berger H, Rebe C, Mary R, Ballot E, Truntzer C, Thibaudin M, Derangère V, Hibos C, Hampe L, et al. Follicular helper-T cells restore CD8 + -dependent antitumor immunity and anti-PD-L1/PD-1 efficacy. J Immunother Cancer. 2021;9(6):2157. doi:10.1136/jitc-2020-002157.

49. Yu D, Rao S, Tsai LM, Lee SK, He Y, Sutcliffe EL, Srivastava M, Linterman M, Zheng L, Simpson N, et al. The transcriptional repressor bcl-6 directs T follicular helper cell lineage commitment. Immun. 2009;31(3):457–468. doi:10.1016/j.immuni.2009.07.002.

50. Petitprez F, de Reyniès A, Keung EZ, Chen TWW, Sun C-M, Calderaro J, Jeng Y-M, Hsiao L-P, Lacroix L, Bougoüin A, et al. B cells are associated with survival and immunotherapy response in sarcoma. Nature. 2020;577(7791):556–560. doi:10.1038/s41586-019-1906-8.

51. Picard E, Verschoor CP, Ma GW, Pawelec G. Relationships between immune landscapes, genetic subtypes and responses to immunotherapy in colorectal cancer. Front Immunol. 2020;11. doi:10.3389/fimmu.2020.00369.

52. Oh DY, Kwek SS, Raju SS, Li T, McCarthy E, Chow E, Aran D, Ilano A, Pai CCS, Rancan C, et al. Intratumoral CD4 + T cells mediate anti-tumor cytotoxicity in human bladder cancer. Cell. 2020;181(7):1612–1625.e13. doi:10.1016/j.cell.2020.05.017.

53. Vanhersecke L, Brunet M, Guégan J-P, Rey C, Bougouin A, Cousin S, Le Moulec S, Besse B, Loriot Y, Larroquette M, et al. Mature tertiary lymphoid structures predict immune checkpoint inhibitor efficacy in solid tumors independently of PD-L1 expression. Nat Cancer. 2021;2(8):794. doi:10.1038/s43018-021-00232-6.

54. Tumeh PC, Harview CL, Yearley JH, Shintaku IP, Taylor EJM, Robert L, Chmielowski B, Spasic M, Henry G, Ciobanu V, et al. PD-1 blockade induces responses by inhibiting adaptive immune resistance. Nature. 2014;515(7528):568–571. doi:10.1038/nature13954.

55. Sui H, Ma N, Wang Y, Li H, Liu X, Su Y, Yang J. Anti-PD-1/PD-L1 therapy for non-small-cell lung cancer: toward personalized medicine and combination strategies. J Immunol Res. 2018;2018:1–17. doi:10.1155/2018/6984948.

56. van Pul KM, Fransen MF, van de Ven R, de Gruijl TD. Immunotherapy goes local: the central role of lymph nodes in driving tumor infiltration and efficacy. Front Immunol. 2021;12:643291. doi:10.3389/fimmu.2021.643291.

57. Posch F, Silina K, Leibl S, Mündlein A, Moch H, Siebenhüner A, Samaras P, Riedl J, Stotz M, Szkandera J, et al. Maturation of tertiary lymphoid structures and recurrence of stage II and III colorectal cancer. Oncoimmunol. 2017;7(2). doi:10.1080/2162402X.2017.1378844.

58. Kasikova L, Rakova J, Hensler M, Lanickova T, Tomankova J, Pasulka J, Drozenova J, Mojzisova K, Fialova A, Vosahlikova S, et al. Tertiary lymphoid structures and B cells determine clinically relevant T cell phenotypes in ovarian cancer. Nat Commun. 2024;151(15):1–19.

59. Mauri C, Menon M. Human regulatory B cells in health and disease: therapeutic potential. J Clin Invest. 2017;127(3):772. doi:10.1172/JCI85113.

60. Dai S, Zeng H, Liu Z, Jin K, Jiang W, Wang Z, Lin Z, Xiong Y, Wang J, Chang Y, et al. Intratumoral CXCL13+CD8+T cell infiltration determines poor clinical outcomes and immunoevasive contexture in patients with clear cell renal cell carcinoma. J Immunother Cancer. 2021;9(2):e001823. doi:10.1136/jitc-2020-001823.

61. de Kleijn S, Langereis JD, Leentjens J, Kox M, Netea MG, Koenderman L, Ferwerda G, Pickkers P, Hermans PWM, et al. Ifn-γ-stimulated neutrophils suppress lymphocyte proliferation through expression of PD-L1. PLoS One. 2013;8(8):72249. doi:10.1371/journal.pone.0072249.

62. He G, Zhang H, Zhou J, Wang B, Chen Y, Kong Y, Xie X, Wang X, Fei R, Wei L, et al. Peritumoural neutrophils negatively regulate

adaptive immunity via the PD-L1/PD-1 signalling pathway in hepatocellular carcinoma. J Exp Clin Cancer Res. 2015;34(1):141. doi:10.1186/s13046-015-0256-0.

63. Wang T, Zhao Y-L, Peng L-S, Chen N, Chen W, Lv Y-P, Mao F-Y, Zhang J-Y, Cheng P, Teng Y-S, et al. Tumour-activated neutrophils in gastric cancer foster immune suppression and disease progression through GM-CSF-PD-L1 pathway. Gut. 2017;66 (11):1900–1911. doi:10.1136/gutjnl-2016-313075.

64. Aloe C, Wang H, Vlahos R, Irving L, Steinfort D, Bozinovski S. Emerging and multifaceted role of neutrophils in lung cancer. Transl Lung Cancer Res. 2021;10(6):2806. doi:10.21037/tlcr-20-760.

65. Zhang C, Tang B, Hu J, Fang X, Bian H, Han J, Hou C, Sun F. Neutrophils correlate with hypoxia microenvironment and promote progression of non-small-cell lung cancer. Bioengineered. 2021;12(1):8872–8884. doi:10.1080/21655979.2021.1987820.

66. Yang R, Wang X, Ma C, Zhang Z, Liu N, Ma X, Zhang Y, Wang X, Liu Y. Tumor-infiltrating neutrophils and peripheral neutrophil-to-lymphocyte ratio conversely predicted the prognosis of patients with non-small cell lung cancer. Cell Immunol. 2022;379:104588. doi:10.1016/j.cellimm.2022.104588.

67. Pillay J, den Braber I, Vrisekoop N, Kwast LM, de Boer RJ, Borghans JAM, Tesselaar K, Koenderman L. In vivo labeling with 2H2O reveals a human neutrophil lifespan of 5.4 days. Blood. 2010;116(4):625–627. doi:10.1182/blood-2010-01-259028.

68. Marsman C, Jorritsma T, Ten Brinke A, van Ham SM. Flow cytometric methods for the detection of intracellular signaling proteins and transcription factors reveal heterogeneity in differentiating human B cell subsets. Cells. 2020;9(12):2633. doi:10.3390/cells9122633.

69. Foundation, R. R: the R project for statistical computing. https://www.r-project.org/.

70. Folcarelli R, Tinnevelt GH, Hilvering B, Wouters K, van Staveren S, Postma GJ, Vrisekoop N, Buydens LMC, Koenderman L, Jansen JJ, et al. Multi-set pre-processing of multicolor flow cytometry data. Sci Rep. 2020;10(1):1–12. doi:10.1038/s41598-020-66195-3.

71. Monaco G, Chen H, Poidinger M, Chen J, de Magalhães JP, Larbi A. flowAI: automatic and interactive anomaly discerning tools for flow cytometry data. Bioinformat. 2016;32 (16):2473–2480. doi:10.1093/bioinformatics/btw191.

72. Hammill D. Interactive analysis of cytometry data • CytoExploreR. 2021. https://dillonhammill.github.io/CytoExploreR/.

73. Finak G, Frelinger J, Jiang W, Newell EW, Ramey J, Davis MM, Kalams SA, De Rosa SC, Gottardo R, et al. OpenCyto: an open source infrastructure for scalable, robust, reproducible, and automated, end-to-end flow cytometry data analysis. PLoS Comput Biol. 2014;10(8):e1003806. doi:10.1371/journal.pcbi.1003806.

74. Van P, Jiang W, Gottardo R, Finak G, Wren J. ggCyto: next generation open-source visualization software for cytometry. Bioinformat. 2018;34(22):3951. doi:10.1093/bioinformatics/bty441.

75. Hahne F, LeMeur N, Brinkman RR, Ellis B, Haaland P, Sarkar D, Spidlen J, Strain E, Gentleman R. flowCore: a bioconductor package for high throughput flow cytometry. BMC Bioinf. 2009;10(1). doi:10.1186/1471-2105-10-106.

76. Finak G, Perez JM, Weng A, Gottardo R. Optimizing transformations for automated, high throughput analysis of flow cytometry data. BMC Bioinf. 2010;11(1). doi:10.1186/1471-2105-11-546.

77. Dai Y, Xu A, Li J, Wu L, Yu S, Chen J, Zhao W, Sun X-J, Huang J. CytoTree: an R/Bioconductor package for analysis and visualization of flow and mass cytometry data. BMC Bioinf. 2021;22(1). doi:10.1186/s12859-021-04054-2.

78. Frank M, Harrell E. Package 'hmisc'. 2023. https://cran.r-project.org/web/packages/Hmisc/index.html.

79. Wickham H. ggplot2: elegant graphics for data analysis. Springer-Verlag New York. 2016.

80. Kay M. Ggdist: visualizations of distributions and uncertainty. Zenodo. 2023; doi:10.5281/ZENODO.10236301.